Redox Biology 19 (2018) 116–133

Contents lists available at ScienceDirect

Redox Biology

journal homepage: www.elsevier.com/locate/redox

Redox-dependent condensation of the mycobacterial nucleoid by WhiB4

Manbeena Chawla[a,1], Saurabh Mishra[a,1], Kushi Anand[a,1], Pankti Parikh[a], Mansi Mehta[a], Manika Vij[b,c], Taru Verma[a,d], Parul Singh[e,f], Kishor Jakkala[a], H.N. Verma[g], Parthasarathi AjitKumar[a], Munia Ganguli[b,c], Aswin Sai Narain Seshasayee[e], Amit Singh[a,*]

[a] Department of Microbiology and Cell Biology, Centre for Infectious Disease Research, Indian Institute of Science, Bangalore 560012, India
[b] Department of Structural Biology, CSIR-Institute of Genomics and Integrative Biology, South Campus, Mathura Road, New Delhi 110020, India
[c] Academy of Scientific and Innovative Research (AcSIR), Anusandhan Bhawan, 2 Rafi Marg, New Delhi 110001, India
[d] Centre for BioSystems Science and Engineering (BSSE), Indian Institute of Science, Bangalore 560012, India
[e] National Centre for Biological Science, Bangalore 560065, India
[f] SASTRA University, Thanjavur 613401, Tamil Nadu, India
[g] Jaipur National University, Jagatpura, Jaipur 302017, India

ARTICLE INFO

Keywords:
Fe-S cluster
Oxidative stress
Nucleoid associated protein
WhiB
Tuberculosis
Mycothiol

ABSTRACT

Oxidative stress response in bacteria is mediated through coordination between the regulators of oxidant-remediation systems (*e.g.* OxyR, SoxR) and nucleoid condensation (*e.g.* Dps, Fis). However, these genetic factors are either absent or rendered non-functional in the human pathogen *Mycobacterium tuberculosis* (*Mtb*). Therefore, how *Mtb* organizes genome architecture and regulates gene expression to counterbalance oxidative imbalance is unknown. Here, we report that an intracellular redox-sensor, WhiB4, dynamically links genome condensation and oxidative stress response in *Mtb*. Disruption of WhiB4 affects the expression of genes involved in maintaining redox homeostasis, central metabolism, and respiration under oxidative stress. Notably, disulfide-linked oligomerization of WhiB4 in response to oxidative stress activates the protein's ability to condense DNA. Further, overexpression of WhiB4 led to hypercondensation of nucleoids, redox imbalance and increased susceptibility to oxidative stress, whereas WhiB4 disruption reversed this effect. In accordance with the findings *in vitro*, ChIP-Seq data demonstrated non-specific binding of WhiB4 to GC-rich regions of the *Mtb* genome. Lastly, data indicate that WhiB4 deletion affected the expression of ~ 30% of genes preferentially bound by the protein, suggesting both direct and indirect effects on gene expression. We propose that WhiB4 structurally couples *Mtb's* response to oxidative stress with genome organization and transcription.

1. Introduction

Mycobacterium tuberculosis (*Mtb*) is the causative agent of tuberculosis (TB), which is one of the major global human health problems. Upon infection, *Mtb* is phagocytosed by alveolar macrophages, where it is exposed to redox stresses such as reactive oxygen and nitrogen species (ROS and RNS) [1,2]. To overcome host-generated redox stress, *Mtb* exploits several resistance mechanisms including alkyl hydroperoxidase, catalase, superoxide dismutases, thioredoxins, glucose-6-phosphate dehydrogenase, methionine-sulfoxide reductase, and the membrane-associated oxidoreductase complex [3,4,5,6,7,8,9].

Apart from these response mechanisms, the bacterial nucleoid also undergoes dynamic changes in its architecture in response to stresses such as ROS, RNS, and changes in osmolarity and pH [10]. Nucleoid-associated proteins (NAPs) including Dps (DNA-binding protein from starved cells) and Fis (Factor for inversion stimulation) in *E. coli*, MrgA (Metallo regulated genes A) in *Staphylococcus aureus*, DR0199 (the homolog of EbfC) in *Deinococcus radiodurans*, HU (the homolog of Hup protein) in *Helicobacter pylori*, and Lsr2 in *Mtb* protect the cells from Fenton-mediated oxidative damage by physically shielding and compacting genomic DNA [11,12,13,14,15]. Whereas regulated condensation of the nucleoid protects the cells against oxidative stress, long-lasting condensation has been shown to perturb normal cellular processes such as replication and transcription and stimulate oxidative stress-mediated death [16]. Despite the recognized importance of bacterial NAPs in modulating the oxidative stress response, the effector proteins that monitor the changes in the cytoplasmic redox potential and sculpt the genome architecture in response to oxidative stress

* Corresponding author.
E-mail address: asingh@iisc.ac.in (A. Singh).
[1] Authors contributed equally to this work.

https://doi.org/10.1016/j.redox.2018.08.006

Available online 13 August 2018

remain unknown. Although *Mtb* NAPs such as HupB (HU) and EspR impact pathogen's survival and virulence, respectively [17,18], whether these proteins organizes chromosome under physiologically-relevant stress conditions is not known. In *Mtb,* several studies have demonstrated the role of redox-responsive WhiB proteins (WhiB1 to WhiB7) in regulating gene expression and controlling a plethora of functions including antibiotic resistance, oxidative/nitrosative/acidic stress response, immune-response, cell division, and secretion [19,20,21,22,23,24,25,26,27–29]. However, several functional aspects of WhiB proteins in *Mtb* have not been investigated. Previously, we have shown that one of the WhiB family member, WhiB4, is required to regulate survival in response to oxidative stress *in vitro* and to regulate virulence *in vivo* [20]. A fundamentally important question remains yet unanswered; what is the mechanism by which WhiB4 coordinates oxidative stress response in *Mtb*? More importantly, while electrophoretic mobility shift assays (EMSAs) revealed DNA binding activity of some of the *Mtb* WhiB proteins [30,27,29], an *in vivo* evidence for redox-dependent DNA binding at a genomic scale using chromatin immunoprecipitation sequencing (ChIP-seq) is still lacking. In this study, we employed multiple analytical techniques to show that WhiB4 dynamically manipulates both DNA architecture and gene expression to control oxidative stress response in *Mtb*.

2. Methods

2.1. Bacterial strains and growth conditions

E. coli cultures were grown in Luria-Bertani (LB) medium (BD Biosciences). When required, the culture medium was supplemented with hygromycin (50 μg ml^{-1} for mycobacteria, 150 μg ml^{-1} for *E.coli*), kanamycin (25 μg ml^{-1} for mycobacteria and 50 μg ml^{-1} for *E.coli*), and ampicillin (100 μg ml^{-1}). For cumene hydroperoxide (CHP, Sigma Aldrich) stress, strains were grown to an exponential phase and exposed to different CHP concentrations. Survival was monitored by enumerating colony forming units (CFU) at 0, 6, 24, and 48 h post-treatment. To examine the influence of WhiB4 over-expression on stress tolerance, *whiB4-OE* strain was grown aerobically till O.D.$_{600}$ of 0.3, induced with 200 ng ml^{-1} Anhydrotetracycline (Atc, Cayman Chemicals) for 24 h at 37°C or as indicated, and exposed to (i) normal aerobic environment, (ii) acidic stress (pH 4.5), and (iii) heat stress (42°C). The growth kinetics was monitored over time by measuring absorbance at 600 nm. Various *Mtb* strains and primers used in this study were listed in Supplementary information Table S6 and S7 and were cultured as described previously [20].

2.2. Microarray experiments

The wt *Mtb*, *MtbΔwhiB4*, and *whiB4-Comp* strains were grown in 7H9 medium supplemented with 1× ADS (Albumin Dextrose Saline enrichment) to an O.D.$_{600}$ of 0.4 and exposed to 0.25 mM CHP for 2 h at 37°C. The experiment was carried out with two biological replicates. At 2 h post-treatment with CHP, total RNA was purified as described [20]. The total RNA was processed and hybridized to the *Mtb* Whole Genome Gene Expression Profiling microarray- G2509F (AMADID: G2509F_034585, Agilent Technologies PLC). DNA microarrays were provided by the University of Delhi South Campus MicroArray Centre (UDSCMAC). RNA amplification, cDNA labeling, microarray hybridization, scanning, and data analysis were performed at the UDSCMAC as described previously [31]. Slides were scanned on a microarray scanner (Agilent Technologies) and analyzed using the GeneSpring software. Results were analyzed in MeV and data was considered significant at $p \leq 0.05$. The normalized data has been submitted to NCBI's Gene Expression Omnibus (GEO, http://www.ncbi.nlm.nih.gov/geo/); accession number GSE73877 and GSE114045.

2.3. qRT-PCR

Total RNA was isolated from logarithmically grown cells of wt *Mtb*, *MtbΔwhiB4 and whiB4-OE* strains and qRT-PCR was performed using gene specific primers (Supplementary information Table S7) as described [20].

2.4. Electrophoretic Mobility Shift Assays (EMSA)

Histidine-tagged version of WhiB4 and its various cysteine mutants were purified by as described elsewhere [20]. The oxidized apo-form of WhiB4 was prepared as described previously [20]. To assess the non-specific DNA binding ability of WhiB4, oxidized apo-WhiB4 was incubated with various DNA molecules in a buffer containing 89 mM Tris, 89 mM boric acid and 1 mM EDTA (pH 8.4) for 30 min. The protein-DNA complexes were resolved on a 1% agarose gel in 1× TBE buffer, stained with ethidium bromide and visualized under UV light. As a control, EMSAs were repeated with a known NAP (histidine tagged HU protein; a kind gift from V. Nagaraja , IISc Bangalore) and a non-NAP transcription factor (histidine-tagged TcrX protein; a kind gift from Deepak K. Saini , IISc Bangalore).

2.5. In vitro transcription assays

Approximately 350 ng of oxidized apo-WhiB4 was incubated with 150 ng of a pGEM plasmid in a final volume of 20 μl, followed by *in vitro* transcription using the Riboprobe *in vitro* Transcription Kit according to the manufacturer's instructions (Promega). Samples were treated with 6% SDS (Amresco Inc.) and 4 mg ml^{-1} proteinase K (Amresco Inc.) for 30 min at 37°C and the reaction products were analyzed on a 1% agarose gel.

2.6. In vivo thiol-trapping analysis

Histidine-tagged WhiB4 was expressed under its native promoter in *MtbΔwhiB4*. At an O.D.$_{600}$ of 0.4, *MtbΔwhiB4* expressing histidine-tagged WhiB4 was treated with 0.1 and 0.5 mM CHP for 24 h. Cultures were treated with 10 mM NEM for 5 min to block the thiol-state of WhiB4. Bacterial pellets were resuspended in lysis buffer [300 mM NaCl, 20 mM Na-Phosphate, 10% Glycerol and 1X protease inhibitor (Amresco Inc.), pH 7.5] and lysed using bead beater (MP Biomedicals). Approximately 30 μg of total cell lysate was resolved by 12% non-reducing SDS-PAGE. Proteins were transferred on to 0.2 μm PVDF membrane and used for Western blot. Western blot analysis was achieved using 1:20,000 dilution of anti-His antibody (GE Life Sciences) for 12 h. The blotted membrane was developed with a 1:20,000 dilution of peroxidase-conjugated anti-mouse IgG (Cell Signaling) and an enhanced chemiluminescence substrate (ECL, Bio-Rad).

2.7. Immuno-blot analysis

The expression of FLAG-tagged version of wt WhiB4 or WhiB4-*cys3* variant was induced using various concentrations of Atc for 16 h. For the immuno-blot assay, bacterial cells were processed as described earlier. WhiB4 was detected using anti-FLAG primary antibody. The blot was developed with enhanced chemiluminescence (ECL, Bio-Rad).

2.8. Atomic force microscopy (AFM)

The oxidized apo-WhiB4 was incubated for 1 min with 7 ng ml^{-1} of supercoiled or relaxed forms of plasmid DNA (pEGFP-C1) in a concentration range from 1:2.5–1:20 (DNA: WhiB4; w/w) at RT and 10 μl of this solution was loaded onto freshly cleaved mica surface. The unbound material was washed with deionised water and the bound surface allowed to air dry. Imaging was carried out using the 5500 scanning probe microscope (Agilent Technologies, Inc.) and the PicoView

software. Images were obtained in tapping mode in the air with 225-mm-long silicon cantilevers (Agilent Technologies) that have a resonance frequency of 75 kHz and a force constant of 2.8 Newton m^{-1}. Scan speed used was one line s^{-1}. Minimum image processing (first order flattening and brightness contrast) was employed. Image analysis was performed using Pico Image software v1.4.4. A similar procedure was adopted for WhiB4-Cys3, *Mtb* HU and *Mtb* TcrX proteins.

2.9. Confocal microscopy

Various *Mtb* strains were grown to exponential phase ($O.D._{600}$ of 0.4) in 7H9 medium and WhiB4 expression was induced as described [20]. Cells were fixed with paraformaldehyde (PFA) and washed with 1X PBS and stained with 4',6-diamino-2-phenylindole (DAPI, 1 μg ml^{-1}, Invitrogen). The bacterial cells were visualized for DAPI fluorescence (excitation at 350 nm and emission at 470 nm) in a Leica TCS Sp5 confocal microscope under a 63X oil immersion objective. Quantification of nucleoid size (larger axis) of 100–150 independent cells was carried out using public domain program OBJECT-IMAGE J. Using these images, relative nucleoid size (RNS) was measured by determining the ratio between length of the nucleoid(s) and the length of the cell by relying on the end points of their larger axes. We only considered cells with bilobed or irregular shaped nucleoid for measurements. For this measurement, we assumed that the width of the nucleoid and that of *Mtb* cells are similar with no significant differences. To calculate RNS, each bacterium was zoomed in and brightness/contrast was adjusted to clearly visualize the contour of nucleoids. After scaling the image to appropriate size using scaling tool, line tool was used to measure the length of the larger axes of nucleoids and cells. Since the images are two-dimensional and *Mtb* cells are small, the value of RNS are merely approximations indicating the trend of compactions or expansion of the nucleoid under conditions studied.

2.10. Immunofluorescence microscopy

The *Mtb*Δ*whiB4* cells overexpressing either FLAG-tagged WhiB4 (*whiB4-OE* strain) or histidine-tagged WhiB4 (His-WhiB4) were fixed with 4% PFA, washed with 1X PBS and permeabilized using 0.1% of Triton-X 100. Cells were blocked with 2% bovine serum albumin (BSA) and incubated with anti-FLAG or anti-His primary antibody. The cells were incubated with anti-mouse IgG Alexa Fluor® 594-conjugated secondary antibody (Invitrogen) followed by staining with DAPI as described earlier. A Leica TCS Sp5 confocal microscope under a 63X oil immersion objective was used for imaging.

2.11. Live dead cell staining

CHP treated cells were washed with 1X PBS and stained using the Live/Dead BacLight Bacterial Viability Kit (Invitrogen). The cells were fixed with 4% PFA and imaged for SYTO9 dye (excitation at 480 nm and emission at 500 nm) and propidium iodide (excitation at 490 nm and emission at 635 nm) in a Leica TCS Sp5 confocal microscope.

2.12. ChIP-Seq

DNA–protein interactions were characterized by cross-linking 100 ml of culture of wt *Mtb* or *whiB4-OE* strains ($O.D._{600}$ of 0.4–0.5) with 1% formaldehyde while agitating cultures at 37 °C for 30 min. Crosslinking was quenched by the addition of glycine to a final concentration of 125 mM. Cells were pelleted, washed in 1X PBS + 1X protease inhibitor cocktail (Sigma), and resuspended in IP Buffer (20 mM K-HEPES pH 7.9, 50 mM KCl, 0.5 mM dithiothreitol and 10% glycerol) + the 1 X protease inhibitor cocktail. Samples were sonicated at high amplitude in a water bath sonicator (Bioruptor, Diagenode) set for 30 s ON & 30 s OFF at 4 °C. Shearing of DNA to an average size of 100–400 bp was confirmed by running a de-crosslinked aliquot on 1% agarose gel. Cell debris was removed by centrifugation and the supernatant was used in the IP experiment. The samples were mixed with buffer IPP150 (10 mM Tris-HCl—pH 8.0, 150 mM NaCl and 0.1% NP40) and immunoprecipitation of FLAG-tagged proteins was initiated by incubating samples overnight rotating at 4 °C with Anti-FLAG® M2 Magnetic Beads (Sigma: M8823). Beads were washed twice with IP buffer and once with Tris-EDTA buffer pH 7.5. Elution was performed in 50 mM Tris–HCl pH 7.5, 10 mM EDTA, 1% SDS for 40 min at 65 °C. Samples were finally treated with RNAse A for 1 h at 37 °C, and cross-links were reversed by incubation for 2 h at 50 °C and for 8 h at 65 °C in elution buffer with Protease K. DNA was purified by phenol-chloroform extraction and quantified. The concentration of the immunoprecipitated DNA was measured using the Qubit HS DNA kit. The resulting ChIP-DNA was subjected to qRT PCR analysis to determine the enrichment in the immunoprecipitated sample (*whiB4-OE*) over the control sample (wt *Mtb*) after normalization with input. Truseq ChIP kit was used for the library preparation. DNA was end-repaired and adapters were ligated. After ligation, products were purified and amplified. Samples were sequenced on the HiSeq. 2500 Sequencing System.

2.13. ChIP- Sequencing analysis

The single end reads obtained were aligned to the reference genome H37Rv (ASM19595v2) using the bwa-0.7.12 version [32]. The tab delimited *.sam* files as output were then converted to .bam format using samtools-1.2 [33]. We then used bedtools2 to convert .bam into .bed files, and both the resultant ChIP and input files in replicates were used in MACS peak calling algorithm (version2) [34,35]. The *p* value cutoff for the peaks was set to be 0.01. Peaks obtained for each condition were visualized in the UCSC microbial genome browser [36]. MEME-ChIP suite (web interface) was used to search for motifs in the WhiB4 peaks [37]. The analysis was also performed using the Z-score approach [38]. This approach assumes normal distribution of the read counts and firstly normalizes the ChIP samples and the corresponding input controls individually with the mode of the distribution. Mode was calculated using the Short function in Genefilter package in R (R Core Team (2016). R: A language and environment for statistical computing (R Foundation for Statistical Computing, Vienna, Austria. URL https://www.R-project.org/) [39] and genefilter: methods for filtering genes from high-throughput experiments. R package version 1.60.0 (https://rdrr.io/bioc/genefilter/). We compared the peaks obtained from both the methods and found ~90% similarity. The GC% was calculated using bedtools2 nuc command, with the default parameters [34]. All the related statistical analyses were performed in R.

Peak coordinates were then intersected with the annotated H37Rv genome. Peaks that were found within 300 base pairs upstream and 50 base pairs downstream of the start sites of the genes were inferred as bound. In parallel, genes were categorized as up-regulated/down-regulated (> = 1.5 $\log_2$ fold change) from the microarray datasets. These bound genes were then overlapped with the up- and down-regulated genes to understand the effect of WhiB4 binding on the regulatory regions and the downstream effects on gene expression.

2.14. Macrophage infections

IFN-ɣ + LPS activated RAW 264.7 macrophages were infected with wt *Mtb* and *whiB4-OE* strains at a multiplicity of infection 10 (MOI 10) of 2 for 4 h, followed by treatment with amikacin to remove extracellular bacteria. After infection, cells were washed thoroughly with warm DMEM medium and resuspended in the same containing 10% FBS. Samples were collected at the indicated time points, lysed using 0.06% SDS-7H9 medium and plated on OADC-7H11 agar medium for CFU determination.

2.15. Transmission electron microscopy

Cells were processed for transmission electron microscopy (TEM), as described previously [40,41]. Cells were prefixed with 1% (w/v) osmium tetroxide buffered in 0.15 M cacodylate buffer (pH-7.2) (Sigma) for 1 h at room temperature. The prefixed cells were then washed once with the same buffer and post fixed for 2 h at room temperature in 0.15 M sodium cacodylate (Sigma) buffer containing 2% (w/v) tannic acid (Sigma) and 2% (v/v) glutaraldehyde (Sigma). Subsequently, the cells were subjected to washing with the same buffer, and were re-fixed in 1% (w/v) osmium tetroxide overnight at 4ºC. Cells were dehydrated in a graded series of ethanol solutions (Merck Millipore) ranging from 20% to 100% with an incubation period of 10 min at each step and finally embedded in LR White resin (Electron Microscopy Sciences) overnight. The embedded samples were then cut with a glass knife using an ultramicrotome by maintaining the section thickness at 70 nm. The sections were stained with 0.5% uranyl acetate (Sigma) and 0.04% lead citrate (Fluka), and observed using FEI Tecnai™ G2 Spirit electron microscope at 120 kV.

2.16. E_{MSH} measurements

Measurements of intrabacterial E_{MSH} during growth *in vitro* and upon exposure to CHP stress were performed as described previously [42].

2.17. Statistical analysis

The overlap was assessed using the GeneOverlap package within R package version 1.6.0 (http://shenlab-sinai.github.io/shenlab-sinai/) and statistical significance was calculated using the Fisher's exact test. GeneOverlap: Test and visualize gene overlaps. R package version 1.6.0.). Chip-Seq data has been submitted to NCBI's Gene Expression Omnibus (GEO, http://www.ncbi.nlm.nih.gov/geo/); accession number GSE100440. Unless otherwise stated all data were graphed and analyzed with Prism v7.0 (GraphPad). Statistical analyses were performed using Student's *t*-tests (two-tailed). Where comparison of multiple groups was made either one-way or two-way ANOVA with Bonferroni multiple comparisons was performed. Differences with a p value of < 0.05 were considered significant.

3. Results

3.1. Mtb WhiB4 regulates gene expression in response to oxidative stress

Previously, we had shown that WhiB4 functions as an autorepressor and marginally influences the expression of 23 genes in *Mtb* under unstressed conditions [20]. Furthermore, a *whiB4* mutant survived better under oxidative stress *in vitro*, in immune-activated macrophages, and was hypervirulent in animals [20]. In agreement with these findings, exposure to increasing concentrations of an oxidant, cumene hydroperoxide (CHP) induced a dose dependent decrease in *whiB4* expression as compared to that of 16s rRNA (Fig. 1A). These findings indicate that the expression of *whiB4* and its regulatory function thereof could be dependent on oxidative stress.

Since the *whiB4* mutant reported earlier retained expression from initial 96 bases [20], we first deleted the entire open reading frame (ORF) encoding WhiB4 in *Mtb* (*MtbΔwhiB4*) (Fig. 1B–D). Next, we performed global transcriptome profiling of wt *Mtb*, *MtbΔwhiB4*, and *whiB4*-complemented (*whiB4-Comp*) strains upon exposure to 0.25 mM CHP. The *whiB4-Comp* strain was constructed by restoring the expression of *whiB4* from its native promoter in *MtbΔwhiB4* [20]. We minimized any influence of oxidative stress-induced cell death on gene expression by performing microarrays at an early time point (2 h) post-CHP treatment. Treatment with CHP influenced the expression of 614 and 429 genes in wt *Mtb* and *MtbΔwhiB4*, respectively, as compared to untreated controls (Supporting information Table S1). First, we analyzed the effect of CHP on wt *Mtb* [2-fold up- and down-regulated, p value ≤ 0.05]. Genes encoding proteins implicated in mitigating oxidative stress such as thioredoxins (*trx*), catalase (*katG*), alkyl hydroperoxidase (*ahpCD*), protein kinase G (*pknG*), isocitrate lyase (*icl*), and Fe-S biogenesis/repair operon (*suf* system) were induced by CHP (Fig. 2 and Supporting information Table S1). Since oxidative stress damages DNA, protein, and lipids, a significant fraction of genes mediating DNA repair, lipids biogenesis, and protein quality control were induced by CHP (Fig. 2). Genes encoding energetically efficient respiratory complexes such as NADH dehydrogenase I (*nuo* operon) were down-regulated, whereas the energetically less favored NADH dehydrogenase type II (*ndh*) and fumarate reductase (*frdB*) were induced in response to CHP (Fig. 2 and Supporting information Table S1). These changes along with the induction of genes associated with the pentose phosphate pathway, glyoxylate shunt, and nicotinamide metabolism involved in maintaining NAD(P)H/NAD^+(P) poise implicate a strategic shift from energy generation to redox balance in response to CHP stress. As expected, oxidative stress triggers the expression of several transcription factors controlling iron homeostasis (*furA* and *ideR*), protein turn-over (*hspR*), and redox homeostasis (*clgR, nrdR, sigE, sigB,* and *sigH*) (Fig. 2). It is known that NAPs, DNA gyrases, and topoisomerases modulate the nucleoid architecture of bacteria in response to oxidative stress [13,43,44]. However, microarray analysis showed that topoisomerase 1 (*topA*) was down-regulated and NAPs such as *espR, lsr2,* and *hupB* were unaffected upon oxidative stress in *Mtb* (Fig. 2 & Supporting information Table S1). It has been reported that *Mtb* displays massive transcriptional changes in response to non-lethal concentrations of another oxidant hydrogen peroxide (H_2O_2; 5–10 mM) [45]. We compared gene expression changes published in response to H_2O_2 (10 mM; 40 min exposure) [45] with the CHP transcriptome. Approximately, ~ 48% of genes induced by CHP also displayed induction upon H_2O_2 treatment, indicating significant similarities between the oxidative stress response induced by H_2O_2 and CHP (Supplementary information Table S1).

Thereafter, we examined the role of WhiB4 in regulating oxidative stress-induced changes in gene expression. To identify genes whose regulation under CHP conditions is influenced by WhiB4, we compared gene expression changes between CHP-treated *MtbΔwhiB4* and CHP-treated wt *Mtb*. We found that the expression of 275 genes was induced and 198 genes was repressed in *MtbΔwhiB4* as compared to that in *wt Mtb* upon CHP-treatment (Supplementary information Table S1). Genes playing overlapping roles in redox-metabolism and central carbon metabolism (CCM) such as *dlaT, bkdC*, *aceE*, *ahpE*, and *ahpCD* were significantly induced in *MtbΔwhiB4* in response to CHP as compared to that in wt *Mtb* (Fig. 2) [46,47,48,49,50,51]. While *nuo* operon was down-regulated in *MtbΔwhiB4* in response to CHP treatment (Supplementary information Table S1), the compensatory increase in the expression of *ndh, frdA,* and cytochrome bd oxidase (*cydAB*) was notably higher in *MtbΔwhiB4* than in wt *Mtb* (Fig. 2 and Supplementary information Table S1). In bacteria, including *Mtb*, cytochrome bd oxidase also displays catalase and/or quinol oxidase activity [52,53], which confers protection against oxidative stress. This is consistent with the higher potential of *MtbΔwhiB4* to tolerate oxidative stress [20], which is further supported by a substantially lesser number of DNA repair genes induced by CHP in *MtbΔwhiB4* as compared to *wt Mtb* (Fig. 2). Several members of the PE-PGRS gene family involved in maintaining cell wall architecture and protection from oxidative stresses were highly expressed in *MtbΔwhiB4* (Fig. 2 & Supplementary information Table S1) [54,55]. Further, *whiB4* deletion increased the expression of transcription factors involved in metal sensing (*kmtR*, *smtB,* and *zur*), antibiotic tolerance (*blaR*), and virulence (*virS*), whereas the expression of *whiB6* was reduced (Fig. 2). In *Mtb* H37Rv, expression and activity of ESX-1 secretion system is linked to regulatory mechanisms involving PhoP, WhiB6 and EspR [21,56,57]. We observed that genes encoding ESX-1, ESX-3, and ESX-4 family members were down-regulated in *MtbΔwhiB4* upon CHP treatment (Fig. 2), indicating a

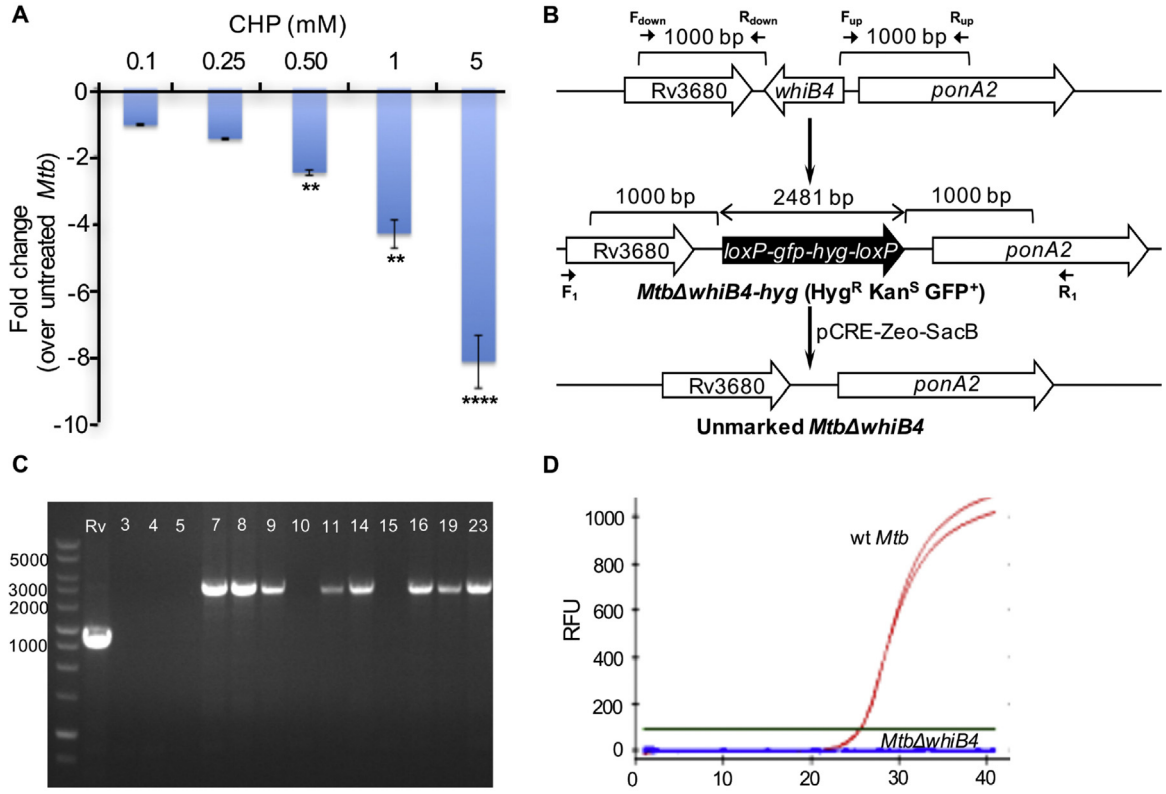

Fig. 1. Oxidative stress downregulates *whiB4* expression in a dose dependent manner. (A) Total RNA was isolated from wt *Mtb* upon treatment with the indicated concentrations of CHP for 2 h. qRT-PCR for *whiB4* was done using *whiB4*-specific oligonucleotides and fold change was normalized to 16 s rRNA expression. Data are represented as mean ± standard deviation (SD). In each experimental condition $n = 3$; two tailed Student's *t*-test was used to determine statistical significance and is indicated where differences were significant. ** p value ≤ 0.01, *** p value ≤ 0.001 (as compared with 0.1 mM CHP treated *wt Mtb*). **(B-D) Generation of *MtbΔwhiB4* knockout in *Mtb*. (B)** A step-wise illustration for construction of an unmarked strain of *MtbΔwhiB4*. Upper right panel denotes wt *Mtb whiB4* loci. After the allelic exchange, entire *whiB4* ORF in *Mtb* genome was replaced by right and left flanking regions of *whiB4* along with the loxP-*hyg-gfp*-loxP cassette. This knock out strain was unmarked by expressing Cre recombinase to remove the *hyg-gfp* cassette. **(C)** Genomic DNA was isolated from putative *MtbΔwhiB4* colonies (7, 8, 9, 11, 14, 16, 19 and 23) which were $Kan^{S}Hyg^{R}GFP^{+}$ and replacement of *whiB4* allele with the Hyg/GFP cassette was confirmed using PCR with F1 and R1 primers (Supplementary information Table S7). An increase in amplicon size from 1.2 kb to 3.3 kb due to insertion of the loxP-*hyg-gfp*-loxP cassette was observed in case of mutant clones, confirming the double crossover event. **(D)** RNA was isolated from logarithmically grown wt *Mtb* and the putative *MtbΔwhiB4* clones. qRT-PCR for *whiB4* was done using *whiB4* specific oligonucleotides (Supplementary information Table S7) and C_t values were plotted to assess the expression. Amplification was detected based on fluorescence emitted by Sybergreen upon interaction with DNA and plotted as Relative Fluorescence Units (RFU).

cross-talk between ESX-associated regulators (*e.g., whiB6/phoP/espR*) and *whiB4*.

Lastly, we determined how many of genes induced or repressed in *MtbΔwhiB4* upon CHP treatment were complemented by the expression of *whiB4*. To do this, we compared wt *Mtb* CHP expression profile with the expression profile of CHP-treated *whiB4-Comp*. We found that expression of ~ 75% of genes showing differential regulation in *MtbΔwhiB4* was normalized to nearly wt *Mtb* levels in the *whiB4-Comp* strain under CHP stress (Fig. 2 and Supplementary information Table S1). For example, differential expression of genes associated with redox metabolism, CCM, PE-PGRS, ESX-systems, and alternate respiration in *MtbΔwhiB4* was significantly stabilized in *whiB4-comp* (Fig. 2 and Supplementary information Table S1). However, expression of ~ 25% of genes remained altered in both *MtbΔwhiB4* and *whiB4-Comp*, indicating the involvement of other genetic factors in regulating their expression upon oxidative stress (Supplementary information Table S1). Lastly, we validated microarray results by measuring the expression of a select set of genes affected by CHP in both wt *Mtb* and *MtbΔwhiB4* by qRT-PCR. As a control, we also examined the expression of genes which were not affected by CHP. As shown in the Table S2, qRT-PCR confirmed differential expression of only CHP-responsive genes in wt *Mtb* and *MtbΔwhiB4*.

3.2. *Mtb* WhiB4 possesses NAP-like DNA binding properties

Having established that WhiB4 influences gene expression upon oxidative stress, we next sought to determine the underlying mechanism. It is known that despite containing redox active 4Fe-4S cluster, WhiB4 binds DNA in the apo-form. Furthermore, the DNA binding of apo-WhiB4 is regulated by the redox state of its cysteine (Cys) residues [20]. The thiol-reduced form of apo-WhiB4 exists as a monomer and lacks DNA binding, whereas oligomeric form of oxidized apo-WhiB4 binds at a specific locus (*ahpCD*) with a poor sequence specificity [20]. The findings, along with the low molecular weight (13.1 kDa) and a highly basic pI (10.28) of WhiB4, are reminiscent of various nucleoid-associated proteins (NAP) (*e.g.,* HNS, HU, IHF and Lrp) [10]. Since oxidative stress caused by CHP exposure is likely to generate oxidized apo-WhiB4 *in vivo*, it is possible that under oxidative conditions WhiB4 influences gene expression by interacting non-specifically with the nucleoid. Using *in vivo* thiol-trapping experiment, we confirmed that WhiB4 largely exists as a monomer of thiol-reduced WhiB4 under normal growing conditions in *Mtb* (Fig. 3B–C and Supplementary information SI Note I). In contrast, exposure to oxidative stress (0.1 and 0.5 mM of CHP) significantly increased the proportion of disulfide-linked dimer (10,000–14,000 molecules) and trimer (4000–6000 molecules) of oxidized apo-WhiB4 per *Mtb* cell (Fig. 3B–C and Supplementary information SI Note I). Next, we investigated

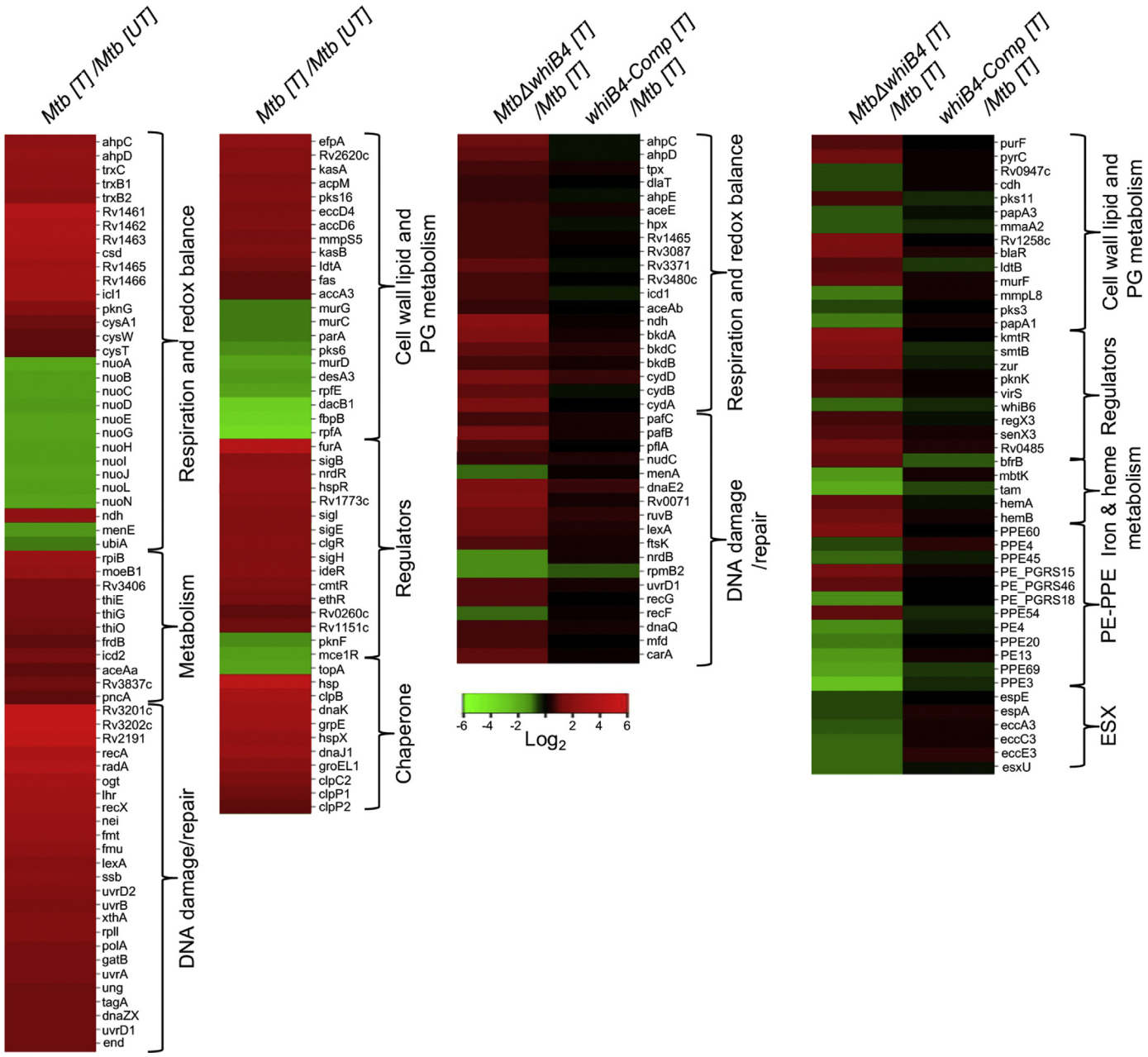

Fig. 2. WhiB4 mediated regulation of gene expression in response to oxidative stress in *Mtb*. Wt *Mtb,* *MtbΔwhiB4,* and *whiB4-Comp* strains were grown and exposed to 250 μM CHP for 2 h. Total RNA was isolated and subjected to microarray analysis. Heat maps depicting the comparison of gene expression (Log_2 fold-change, p value ≤ 0.05) coordinating respiration, CCM, DNA damage, PE-PPE and redox balance between wt *Mtb* [T] vs wt *Mtb* [UT]; *MtbΔwhiB4* [T] vs *wt Mtb* [T] and *whiB4-Comp* [T] vs *wt Mtb* [T] from two biological samples. UT- untreated, T- CHP treated.

whether oxidized apo-WhiB4 possesses a NAP-like DNA binding properties *in vitro* and inside *Mtb*. Similar to other bacterial NAPs [11,10], the oxidized apo-WhiB4 formed a high molecular weight complex with a range of DNA substrates (*e.g.,* supercoiled DNA, linearized DNA, and 1 kb λ DNA ladder) and inhibited transcription from a standard T7-promoter of pGEM plasmid *in vitro* (Fig. 4A–C). The inclusion of the thiol-reductant, dithiothreitol (DTT), or replacement of any cysteine residues with alanine in WhiB4, reversed the DNA binding and transcriptional inhibitory activities of oxidized apo-WhiB4 (Fig. 4D-E). As controls, we showed that a well-established NAP (*Mtb* HU, Rv2986c [17]) forms a high molecular weight complex with a supercoiled DNA or a 1 kb λ DNA ladder, whereas a non-NAP transcription factor (*Mtb* TcrX, Rv3765c [58]) remained ineffective (Fig. 4F–G). In contrast to WhiB4, addition of DTT did not influence the activities of HU or TcrX in these assays (Fig. 4H–I).

Further, we examined apo-WhiB4 DNA binding properties using Atomic Force Microscopy (AFM). A super-coiled plasmid DNA (pEGFP-C1) was pre-exposed to increasing concentrations of oxidized apo-WhiB4 and subjected to AFM. The oxidized apo-WhiB4 and plasmid DNA were taken as the experimental controls. AFM images in the absence of WhiB4 showed uniform structure for the negatively super-coiled plasmid DNA (Fig. 5A). Interestingly, at lower amounts of oxidized apo-WhiB4, a gradual relaxation of supercoiled plasmid DNA with initial opening at the ends, followed by a mixed population of partially or fully opened DNA circles was detected (Fig. 5B–C). Further increase in oxidized apo-WhiB4 resulted in the formation of multiple loops, bends and condensation within a single DNA molecule (Fig. 5D–F). A further increase in the protein concentrations may lead to nucleoprotein filament formation. However, higher concentrations of oxidized apo-WhiB4 forms large aggregates on the mica surface, thus

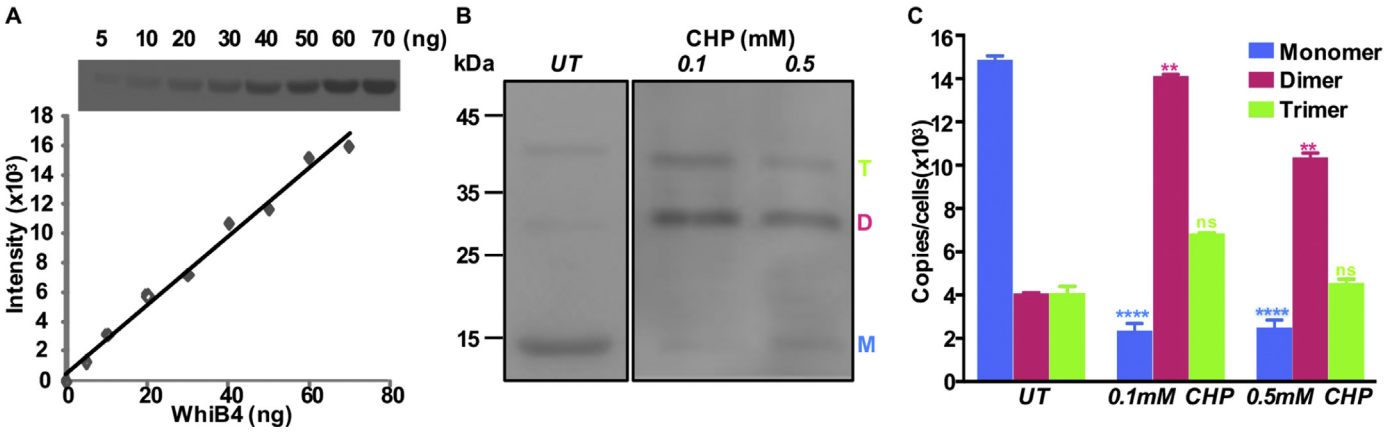

Fig. 3. CHP stress induces the generation of oxidized apo-WhiB4 oligomers *in vivo*. (A) Indicated concentrations of purified histidine-tagged WhiB4 were subjected to immuno-blot analysis using anti-His antibody. Band intensities were quantified by Image J and plotted to generate a standard curve. **(B)** *MtbΔwhiB4* expressing chromosomally-integrated histidine-tagged WhiB4 from native promoter were grown till an OD_{600} nm of 0.8, harvested, and cell free extract was analyzed for monitoring expression and oligomerization of WhiB4 under normal growing conditions and upon exposure to 0.1 and 0.5 mM of CHP for 24 h. To minimize the possibility of O_2-induced thiol oxidation and subsequent oligomerization of apo-WhiB4 during cell-free extract preparation, cells were pre-treated with the thiol-alkylating agent NEM as described [20]. Approximately 30 µg of the cell-free extract was resolved on a 12% non-reducing SDS-PAGE and immuno-blotted using anti-his. (C) The band intensities were calculated using Image J and compared with the standard curve to calculate the amount of WhiB4 expressed inside a single Mtb cell. These values were converted to WhiB4 copies per cell as described in Materials and Methods and plotted. Data shown are the representatives of two independent experiments. The asterisk (**P < 0.01/****P < 0.0001) represents a significant difference in the band intensity of monomer and dimer between UT and treated using One-way ANOVA with Bonferroni's post hoc test. M: monomer, D: dimer, T: trimer.

precluding any further AFM imaging. An assessment of various geometric properties of the imaged protein: DNA complexes confirmed an initial increase in diameter and length followed by a decrease in both parameters at higher protein concentrations (Fig. 5G). This dual compactional ability of WhiB4 indicates a stoichiometry-dependent regulatory role for WhiB4, as shown for other chromosomal architectural proteins HU and RdgC in *E.coli* [59,60,61]. The Cys3-WhiB4 (replacement of the third cysteine to alanine) mutant protein was unable to exhibit a similar effect on supercoiled pEGFP-C1 (Supplementary information Fig. S1), indicating that WhiB4 Cys residues function as a thiol-based redox switch that modulates DNA condensing activity. Lastly, similar to apo-WhiB4, *Mtb* HU initially relaxed supercoiled pEGFP-C1 at a lower concentration followed by extensive DNA compaction at higher concentrations (Supplementary information Fig. S2). As expected, *Mtb* TcrX did not influence DNA architecture (Supplementary information Fig. S2).

3.3. WhiB4 condenses the mycobacterial nucleoid

To further understand the link between DNA condensation and WhiB4, we examined the nucleoid morphology of wt *Mtb*, *MtbΔwhiB4*, *whiB4-Comp,* and *whiB4-OE* strains. The *whiB4-OE* strain overexpresses FLAG-tagged WhiB4 from an anhydrotetracycline (Atc)-inducible promoter system [20]. As controls, we similarly overexpressed *Mtb* HU (*HU-OE*) and *Mtb* TcrX (*TcrX-OE*). We stained the nucleoids of various strains with 4',6-diamidino-2-phenylindole (DAPI) and visualized the cells by confocal microscopy. DAPI stained cells from exponentially grown cultures of *Mtb* frequently showed the presence of expanded nucleoids with a fewer bilobed nucleoid. Infrequently, single cells containing more than 3 distinct DAPI stained regions were also observed. Using these images we measured relative nucleoid size (RNS) by determining the ratio between the length of the nucleoid(s) and the length of the cell by relying on the end points of their larger axes (region with see Methods). Since the images are two-dimensional and cells are small, the values of RNS are merely approximations indicating the trend of compactions or expansion of the nucleoid under conditions studied. The differences in RNS values across multiple samples and assay conditions were comprehensively analyzed for significance using ANOVA followed by multiple post-hoc adjustment tests (Bonferroni, Sidak, and Tukey's). Please refer to Supplementary information Table S3 for a complete list of *p* values.

Wt *Mtb*, *MtbΔwhiB4,* and *whiB4-Comp* showed expanded nucleoids with a slightly higher RNS value for *MtbΔwhiB4* (Fig. 6 and Supplementary information Fig. S3). Overexpression of WhiB4 resulted in a significant compaction of the nucleoid (Fig. 6 & Supplementary information Fig. S3). The mean RNS value reduced by ~ 50% (0.125 ± 0.002 µm) in case of *whiB4-OE* as compared to wt *Mtb* (0.261 ± 0.005 µm, *p* value < 0.0001) or *MtbΔwhiB4* (0.291 ± 0.005 µm, *p* value < 0.0001). Overexpression of HU induced compaction similar to WhiB4 (mean RNS = 0.120 ± 0.002 µm), whereas the nucleoid remained expanded upon TcrX overexpression (mean RNS = 0.265 ± 0.007 µm) (Fig. 6 and Supplementary information Fig. S3). Over-expression of untagged WhiB4 also condensed the mycobacterial nucleoid, ruling out the influence of the FLAG-tag on genome compaction (Supplementary information Fig. S4). Further, our intracellular localization studies using FLAG-specific antibody followed by indirect immuno-fluorescence revealed that WhiB4 is associated with the DAPI-stained clumped nucleoids of *whiB4-OE* (Fig. 7A). In contrast, over-expression of the cysteine mutant of WhiB4 (*whiB4-cys3-OE*) did not induce DNA condensation (mean RNS = 0.255 µm ± 0.046, *p* value < 0.001 as compared to *whiB4-OE*), and the mutant protein was found scattered across the length of the cell (Fig. 7A–B). Overall expression of WhiB4 was maintained in the *whiB4-cys3-OE* strain, indicating that the loss of nucleoid condensation is likely due to disruption of the thiol-disulfide redox switch (Fig. 7C).

We substantiated WhiB4-induced nucleoid condensation by performing ultrastructure imaging of the mycobacterial nucleoid using Transmission Electron Microscopy (TEM). Analysis of mid-logarithmic (log) phase cells overexpressing WhiB4 showed a highly condensed nucleoid, unlike the well spread out nucleoid in the wt *Mtb* cells, *MtbΔwhiB4*, and *whiB4-Comp* (Fig. 8, compare C-D with A-B, E-F, & G-H, respectively). The nucleoid morphology of the wt *Mtb* cells was as reported previously [62,40,63]. Similar to *whiB4-OE*, TEM of HU overexpressing strain showed a highly compacted nucleoid, whereas *TcrX-OE* displayed nucleoid architecture comparable to wt *Mtb* (Fig. 8I-L).

A broadly comparable nucleoids of wt *Mtb*, *MtbΔwhiB4,* and *whiB4-Comp* suggests a negligible effect of WhiB4 on DNA condensation under normal growing conditions. This is in agreement with our *in vivo* thiol-

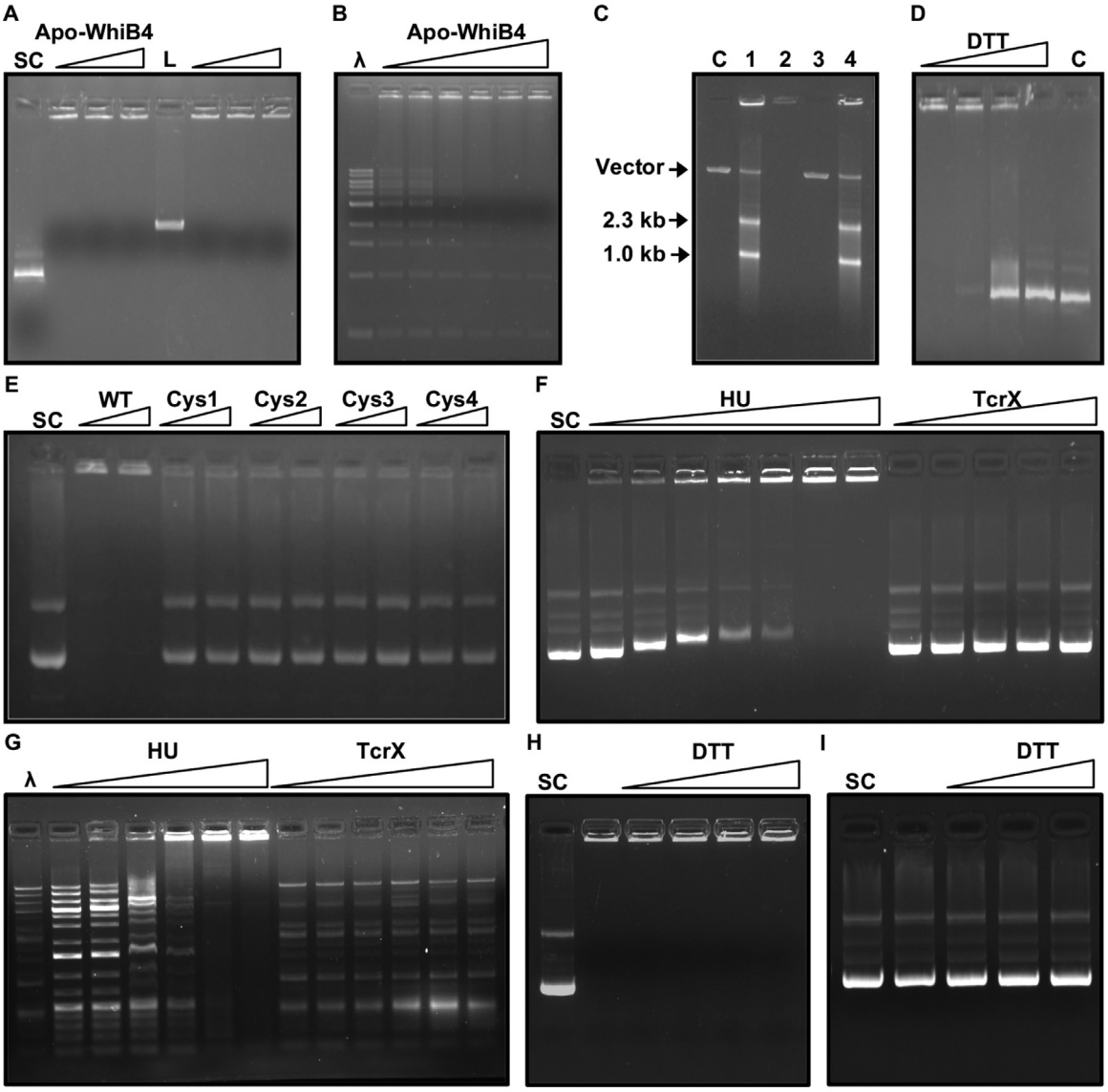

Fig. 4. *Mtb* WhiB4 exhibits non-specific DNA binding activities. (A) 150 ng of either linear (L) or supercoiled (SC) plasmid DNA was incubated with oxidized apo-WhiB4 (250 ng [lanes 2, 6]; 300 ng [lanes 3, 7]; 350 ng [4, 8]). Lanes 1 and 5 represent DNA without WhiB4. **(B)** Binding of apo-WhiB4 (100, 150, 200, 250, 300 and 350 ng) with 1 kb λ-DNA ladder (λ) (150 ng). **(C) WhiB4 represses transcription**. *In vitro* transcribed pGEM plasmid in the absence of apo-WhiB4 (lane 1), oxidized apo-WhiB4 in complex with pGEM (lane 2), *in vitro* transcription of pGEM in the presence of oxidized (lane 3) or reduced (lane 4) apo-WhiB4. The reactions in lane 3 and 4 were treated with 6% SDS and 4 mg ml^{-1} protease K to remove WhiB4 from the mixture before separation. C: pGEM plasmid DNA alone. **Cysteine residues regulate DNA binding of WhiB4 (D)** DTT-treatment abolished DNA binding of WhiB4. Oxidized apo-WhiB4 (350 ng) was treated with DTT (0, 200, 400, 800 mM) for 2 h followed by binding to the supercoiled plasmid DNA. C: represents DNA without WhiB4. **(E)** Purified wt apo-WhiB4 and Cys mutant variants were treated with thiol oxidant, diamide, and the gel-shift assay was performed as described earlier. DNA binding assays using *Mtb* HU (50–350 ng) and *Mtb* TcrX (150–350 ng) with **(F)** supercoiled DNA and **(G)** 1 kb λ-DNA ladder. **(H)** 350 ng of *Mtb* HU or (I) *Mtb* TcrX were treated with increasing concentrations of DTT (0, 200, 400, 800 mM) for 2 h followed by binding to the supercoiled plasmid DNA. The samples were analyzed on 1% agarose gel.

trapping data showing that only a minor fraction of WhiB4 exists in a DNA-condensing redox form (*i.e.* oxidized apo-WhiB4 dimer/trimer) *in vivo* under native conditions. In contrast, a highly compacted nucleoid of *whiB4-OE* indicates the accumulation of DNA condensing oligomeric forms of oxidized apo-WhiB4 upon WhiB4 overexpression. To explore this, we performed *in vivo* thiol-trapping experiment upon Atc-mediated WhiB4 induction. We found that induction with 100 ng ml^{-1} of Atc resulted in ~ 14,000 dimers and 4000 trimers of disulfide-linked oxidized apo-WhiB4 per cell (Fig. 9 and Supplementary information SI Note II). The proportion of dimers and trimers were comparable to the oxidized apo-WhiB4 forms generated in *Mtb* upon treatment with 0.1–0.5 mM CHP. Since oxidized apo-WhiB4 functions as an autorepressor and also as a repressor of antioxidant systems [20], it is conceivable that the overexpression of WhiB4 by Atc circumvents this autoregulatory loop to amplify the negative effect of WhiB4 on antioxidants expression. Consequently, oxidative stress increases inside *Mtb*, resulting in oxidation of WhiB4 thiols to generate disulfide-linked oxidized apo-WhiB4 oligomers. Altogether, using multiple analytical techniques, we confirmed that WhiB4 participates in mycobacterial nucleoid compaction in a redox-dependent manner.

3.4. WhiB4 regulates DNA condensation in response to oxidative stress

Having shown that WhiB4 modulates nucleoid condensation, we wanted to understand the influence of oxidative stress on mycobacterial nucleoids and the role of WhiB4 in this outcome. We treated wt *Mtb*, *MtbΔwhiB4,* and *whiB4-OE* strains with 0.5 mM CHP and monitored intramycobacterial oxidative stress, nucleoid condensation, and

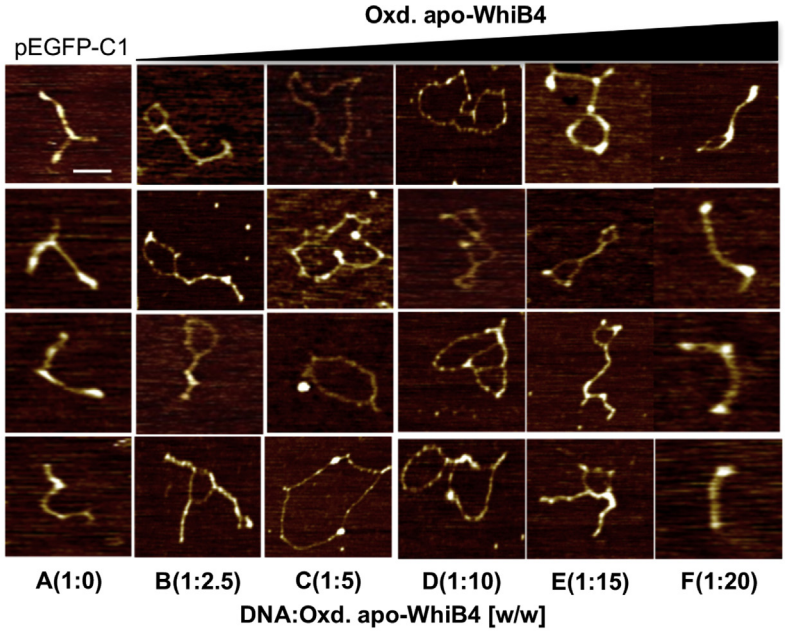

Fig. 5. AFM analysis of WhiB4-mediated DNA condensation. (A) Supercoiled plasmid DNA, **(B-F)** Oxidized apo-WhiB4 incubated with supercoiled plasmid in increasing concentration (DNA: protein w/w =1:2.5, 1:5,1:10,1:15, and 1:20). **(B and C)** Low protein to DNA ratio gradually opens up the DNA until a fully relaxed circular DNA molecule is formed as observed in the case of a moderate protein to DNA ratio**. (D and E)** Further increase in protein to DNA ratio reverses the phenomenon when lateral compaction occurs. **(F)** High protein to DNA ratio further causes condensation of the DNA molecules thereby leading to rigid filamentous structures. The scale of images is 0.8 μm × 0.8 μm, Scale bar is 100 nm. **(G)** Geometric properties of the imaged protein: DNA complexes. Geometrical parameters of supercoiled DNA in the absence and presence of oxidized apo-WhiB4. (A- DNA only, B- low protein to DNA ratio, C-E- moderate protein to DNA ratio, F- high protein to DNA ratio; n = 70 independent DNA molecules measured in each case). Data are represented as mean ± SEM.

G

Parameter (nm)	DNA:Oxd apo-WhiB4 **(1:0)**	DNA:Oxd apo-WhiB4 **(1:2.5)**	DNA:Oxd apo-WhiB4 **(1:5)**	DNA:Oxd apo-WhiB4 **(1:10)**	DNA:Oxd apo-WhiB4 **(1:15)**	DNA:Oxd apo-WhiB4 **(1:20)**
Length	383± 49	723± 78.4	1249± 157	932.12±9	536±52	458±64
Width	29± 3.2	20.6± 2.3	15.7± 1.32	18.48±1.9	21.77±2.1	26.58±2.9
Diameter	29± 3.2	152± 16	365± 39.5	196±23	93.25±8.9	26.58±2.9

survival at various time points. To image oxidative stress in *Mtb*, we measured the redox potential of its most abundant cytoplasmic thiol (mycothiol; MSH) using Mrx1-roGFP2. The biosensor shows an increase in fluorescence excitation ratio at 405/488 nm upon oxidative stress, whereas a ratiometric decrease is associated with reductive stress [5]. The ratiometric changes (405/488 nm) in the fluorescence of the biosensor can be fitted to the modified Nernst equation to precisely determine the millivolt (mV) changes in the redox potential of mycothiol (E_{MSH}) [42].

Under unstressed conditions, both wt *Mtb* and *MtbΔwhiB4* displayed a steady-state E_{MSH} of ~ −276 mV. However, overexpression of WhiB4 induces an oxidative shift in E_{MSH} of *whiB4-OE* (~ −250 mV), consistent with the antioxidant repressor function of WhiB4. Treatment with 0.5 mM CHP induces a significant oxidative shift in E_{MSH} of wt *Mtb* (-220 to −225 mV) at 6 h and 24 h post-treatment (Fig. 10A). Importantly, the nucleoids of wt *Mtb* underwent a noteworthy condensation at 6 h (mean RNS: 0.14 μm ± 0.02, p value < 0.001 as compared to 0 h) and 24 h (mean RNS: 0.10 μm ± 0.01, p value < 0.001) post-treatment (Fig. 10A). At 48 h post CHP-treatment, cells showed loss of DAPI fluorescence and appeared rounded/irregular, thus precluding any measurements of nucleoid length. These morphological alterations are indicative of DNA fragmentation and complete killing, which we confirmed by CFU analysis (Fig. 10B) and SYTO9-propidium iodide staining (Fig. S5). We expressed *whiB4* fused with histidine-tag (His-tag) and examined colocalization of HIS-WhiB4 with DAPI stained nucleoids under CHP stress. Using His-tag antibody and indirect immunofluorescence, we confirmed that WhiB4 remained associated with the condensed nucleoid upon CHP exposure at 6 h and 24 h post-treatment (Fig. 11). Notably, the skew towards condensed DNA and oxidative E_{MSH} was activated at a time point where toxicity was modest (*i.e.* 6 h), indicating that genome hypercompaction likely precedes oxidative stress-induced killing of *Mtb*.

In comparison to wt *Mtb*, nucleoids of *MtbΔwhiB4* underwent a slower transition towards a condensed state, which corresponds to a moderate shift towards oxidative E_{MSH} (E_{MSH}: -247 to − 239 mV) and a slower killing by CHP (Fig. 10A–B). The degree of condensation displayed by *MtbΔwhiB4* at 48 h of CHP treatment (RNS = 0.118 ± 0.02) was similar to that observed in case of wt *Mtb* (RNS = 0.104 ± 0.01) at 24 h post CHP-treatment. Similarly, while *MtbΔwhiB4* was successful in maintaining intermediate degree of oxidative E_{MSH} (-239 mV) and survival, wt *Mtb* displayed acute oxidation and killing at 48 h post-CHP treatment (Fig. 10A–B). However, the fact that *MtbΔwhiB4* exhibited nucleoid compaction (albeit slower) in response to CHP suggests that WhiB4 is involved in mediating appropriate degree of DNA condensation perhaps with the involvement of one or more partner NAPs under oxidative conditions. In *whiB4-OE*, 0.5 mM CHP treatment for 6 h was sufficient to induce substantial DNA condensation (mean RNS = 0.06 μm ± 0.01), overwhelm redox balance (E_{MSH}: −225 mV ± 0.98) and induce substantial killing (Fig. 10A–B). At 24 and 48 h, CHP induces complete killing of *whiB4-OE,* precluding further measurements of RNS (Fig. 10B).

It can be argued that the high concentration of CHP (0.5 mM) can adversely affect *Mtb's* physiology to influence genome topology. To address this issue, we reassessed nucleoid condensation, intrabacterial E_{MSH}, and survival upon exposure to a non-toxic concentration of CHP (0.1 mM) over time. As expected the effect of 0.1 mM CHP was moderate, however, the relative differences in RNS, E_{MSH}, and survival between wt *Mtb*, *MtbΔwhiB4*, and *whiB4-OE* followed a pattern similar to 0.5 mM CHP (Supplementary information Fig. S6 & SI Note III). Finally, to examine if the hypersensitivity to oxidative stress is unique to WhiB4 overexpression, we monitored survival of *HU-OE* and *TcrX-OE* in response to 0.1 mM CHP. In contrast to *whiB4-OE*, survival of *HU-OE* and *TcrX-OE* was not significantly affected by CHP (Supplementary information Fig. S7), indicating that WhiB4 directed changes in genome condensation and expression calibrate survival upon CHP stress.

Since our results indicate an inverse relationship between genome

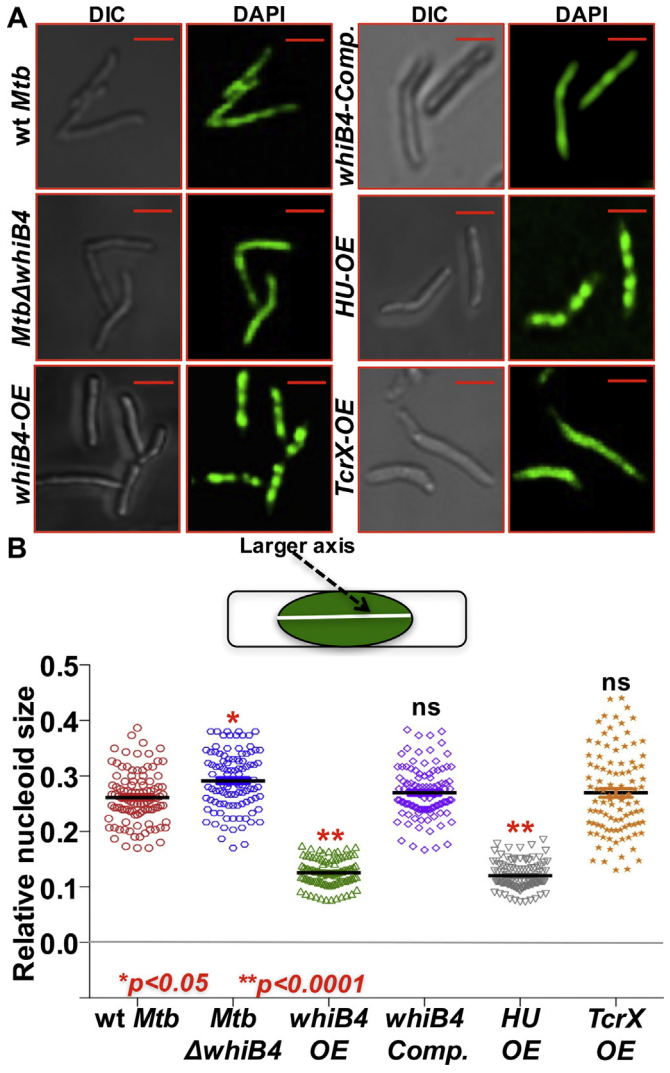

Fig. 6. WhiB4-mediated nucleoid compaction in *Mtb*. **(A)** Nucleoid of wt *Mtb*, *MtbΔwhiB4*, *whiB4-OE, whiB4-Comp*, *HU-OE and TcrX-OE* strains were stained with DAPI (pseudo colored green) and visualized under confocal microscopy (63X). **(B)** Relative Nucleoid Size (RNS) (larger axis; *inset*) of ~ 100–150 independent cells of various *Mtb* strains. For overexpression, 100 ng ml^{-1} of Atc was added to cultures. As a control, the same amount of Atc was added to other strains. Scale bar = 2 μm. Data shown are the average of two independent experiments done in triplicate. Results are expressed as Mean ± SEM. One-way analysis of variance (ANOVA) with Bonferroni's post hoc test was employed to determine statistical significance between the RNS of different strains. Comparisons in which p value is < 0.05 were indicated with the symbol (*). Symbol: comparison to wt *Mtb*.

condensation and survival under oxidative stress, we examined the state of nucleoids in a *Mtb* strain completely devoid of MSH antioxidant (*MtbΔmshA*) and in a *mshA* complemented strain (*mshA-comp*) [64]. Similar to *whiB4-OE*, *MtbΔmshA* grows normally under aerobic conditions but shows oxidative E_{MSH} and acute sensitivity towards oxidative stress [65]. In agreement to findings with *whiB4-OE*, nucleoids of *MtbΔmshA* cells showed hypercondensation (mean RNS: 0.11 μm ± 0.04) as compared to the *mshA-comp* cells (mean RNS: 0.25 μm ± 0.02) (Supplementary information Fig. S8) under normal growing conditions. These results reinforce a functional association between DNA condensation and tolerance to oxidative stress in *Mtb*. In summary, our data indicate that deletion of WhiB4 reduces, and overexpression potentiates, the adverse impact of DNA condensation on oxidative stress survival.

3.5. ChIP-Seq demonstrates a nearly-uniform association of WhiB4 with Mtb chromosome

To determine genome-wide distribution of oxidized apo-WhiB4, we performed ChIP-Seq. The oxidized apo-WhiB4 can be generated by CHP treatment *in vivo*, however this form of WhiB4 functions as an autorepressor and therefore can pose challenges in identifying transient binding sites. To circumvent this, we utilized *whiB4-OE*, which consistently generates oxidized apo-WhiB4 to perform ChIP-Seq. We considered the possibility that ectopic expression might result in non-physiological DNA binding. However, our data showed that overexpression of WhiB4 using 100 ng ml^{-1} of Atc produced nearly physiological concentrations of oxidized apo-WhiB4 molecules/cell (comparable to CHP treated *Mtb*). Furthermore, using qRT-PCR we confirmed that overexpression of FLAG-tagged or untagged WhiB4 influences the expression of only WhiB4-specific genes (Supplementary information Table S2). Further, *whiB4-OE* displayed survival defects exclusively under oxidative stress conditions *in vitro* and inside immune-activated macrophages (Fig. 12 and SI Note IV). Lastly, recent studies have demonstrated remarkable consistency between the DNA binding profile of several ectopically overexpressed FLAG-tagged transcription factors and ChIP-Seq studies performed under native conditions in *Mtb* [66]. Thus, while we cannot exclude the possibility that overexpression could lead to nonphysiological DNA binding, we conclude that WhiB4 overexpression did produce physiologically-relevant redox-form(s) necessary for DNA binding in *Mtb*.

We induced the expression of WhiB4 using 100 ng of Atc for 16 h in duplicate, harvested chromatin samples for ChIP-Seq using anti-FLAG antibody conjugated to magnetic beads, and sequenced the cross-linked DNA using the Illumina Genome Analyzer system. As a negative control, we sequenced the input chromatin sample prior to immunoprecipitation (IP) with the anti-FLAG antibody. In parallel, we performed the analysis of a published genome-wide DNA binding study that was conducted using a sequence-specific transcription factor CRP in *Mtb* [67]. Since the ChIP-seq data for *Mtb* HU are not available, we analyzed genome-wide DNA binding data of *E.coli* HU as an exemplar of a near-uniform DNA binding protein [68]. For each sample, we examined read count distribution by measuring the number of reads mapped to each base on the chromosome and then plotted the densities of read count distributions. The numbers of reads mapping to each position on the chromosome were first normalized to Z-scores as described previously [68], and represented as density distribution curves (Fig. 13). The normalization is based on the assumption that the noise in the ChIP experiment follows a normal distribution. The Z-score for the signal at any position on the chromosome is defined by the difference between the signal at that position and the mean of the normal noise distribution, divided by the standard deviation of the normal noise distribution. The distribution for data generated from input DNA sequencing shows a peak, whose position depends on the sequencing depth, and a short right hand tail (Fig. 13). The equivalent distribution for a highly specific DNA binding protein such as *Mtb* CRP shows a sharp peak to the left, corresponding to the background, and a long right handed tail corresponding to strong DNA binding signals (Fig. 13). A near-uniform DNA binding protein, such as HU in *E. coli*, displays a peak that is largely similar to the input, but with a slight right tail corresponding to regions of weak binding specificity (Fig. 13). Analysis of WhiB4 ChIP-seq resulted in a density distribution curve that showed similarity to input/HU with a slightly more prominent right tail corresponding to regions of weak DNA binding (Fig. 13). The length of the tail can be visually appreciated, and can be quantified using a standard statistical parameter, skewness; higher the skewness, more prominent the tail (Fig. 13 showing higher skewness for CRP than WhiB4). For clarity, we also plotted the Z-score distribution (Z-score > 3) within the right hand tail region (enriched regions of DNA binding) for ChIP experiments for WhiB4, CRP, and *E. coli* HU. In comparison to corresponding inputs, Z-score distributions were weakly skewed to the right

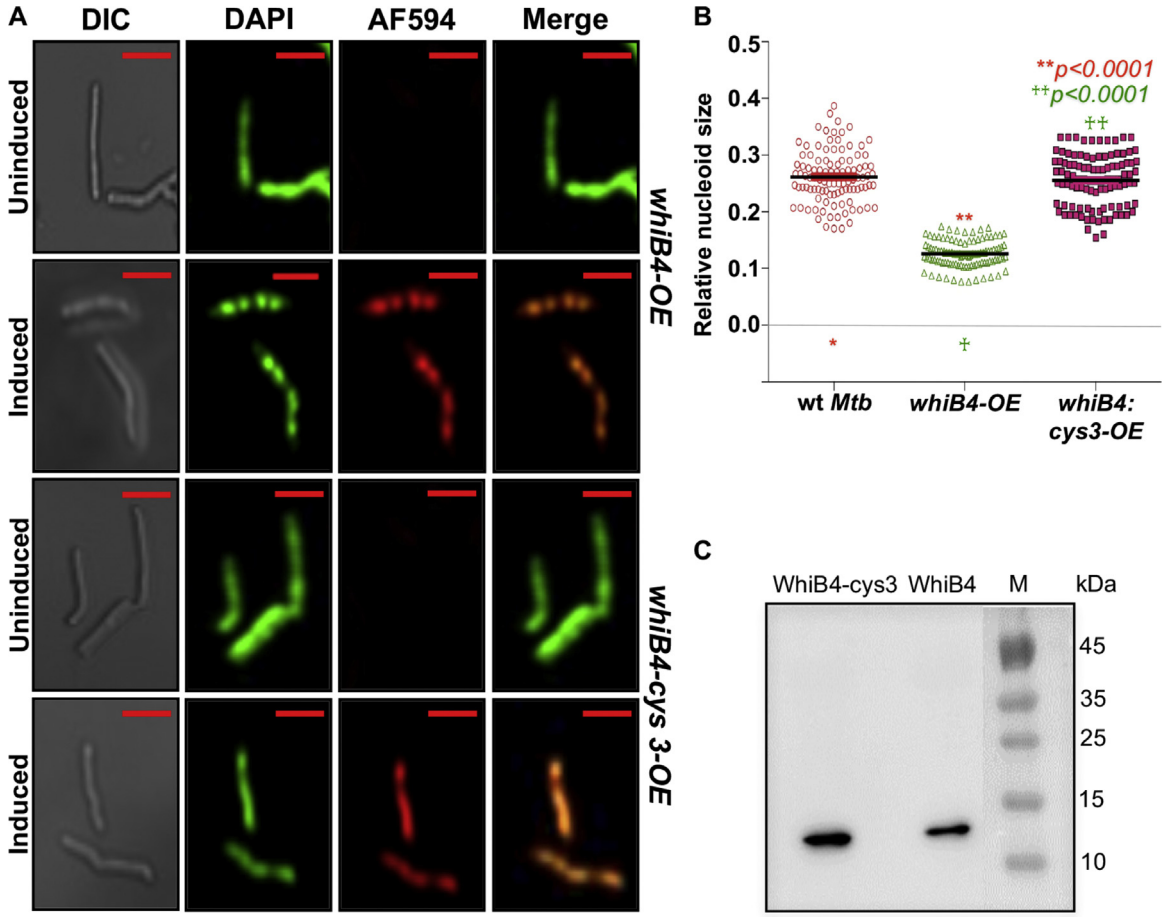

Fig. 7. Cysteine residues of WhiB4 are important for its DNA condensation activity. (A) Confocal microscopic images (63X) of *MtbΔwhiB4* strain over-expressing WhiB4- and WhiB4-cys3 FLAG tagged proteins. Nucleoids were stained with DAPI (pseudo colored green), wt WhiB4-FLAG and WhiB4-cys3-FLAG mutant were stained with the AF594 secondary antibody (red) against the anti-FLAG primary antibody, and co-localization was indicated by yellow in the merge panel. For inducing WhiB4, 100 ng ml^{-1} of Atc was added to cultures of *whiB4-OE and whiB4-cys3* strains. The uninduced (UI) control lacks immuno-fluorescence due to the absence of WhiB4 expression. The scale bar = 3 μm. **(B)** The RNS values of ~ 100-150 independent cells of various *Mtb* strains. Results are expressed as mean ± SEM. The significance of differences between the strains were determined by one-way ANOVA with Bonferroni's post hoc test. Comparisons whose *P* value is < 0.05 were indicated with different symbols. Symbols: (*): comparison to wt *Mtb*; (□): comparison to *whiB4-OE*. **(C)** 30 μg of cell free extract from either *whiB4-OE* or *whiB4-cys3-OE* strains was analyzed for the WhiB4 expression by immuno-blotting using the antibody against FLAG tag. The figure shown is the representative image of two independent experiments.

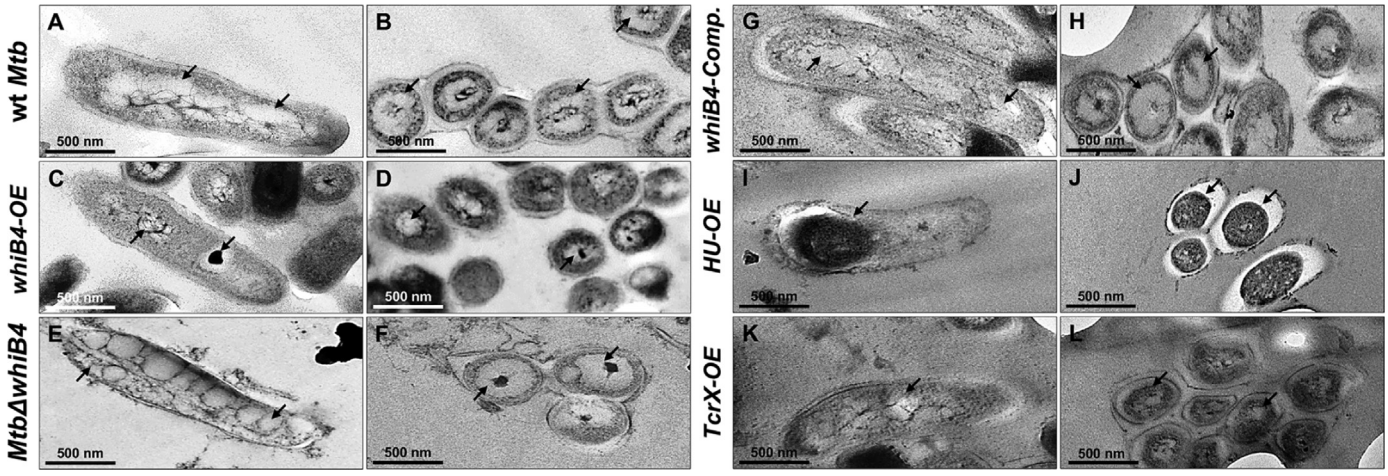

Fig. 8. Transmission electron microscopic (TEM) analysis of *Mtb* nucleoids. TEM images of the longitudinal and transverse sections of: **(A, B)** wt *Mtb* from mid-log phase culture showing a well spread out nucleoid in the middle of the cell; **(C, D)** *whiB4-OE* cells showing highly condensed nucleoid in the middle of the cell; **(E, F)** *MtbΔwhiB4* showing unorganized and well spread out nucleoid throughout the cell; **(G, H)** *whiB4-comp* showing nucleoid like wt *Mtb* (**A, B**). **(I, J)** *HU-OE* showing highly condensed nucleoid, and **(K, L)** *TcrX-OE* showing a well spread nucleoid. Arrowhead indicates nucleoid. For induction, 100 ng ml^{-1} of Atc was used. As a control, the same amount of Atc was added to other strains. In each case, ~250–300 independent cells were visualized and representative images are shown.

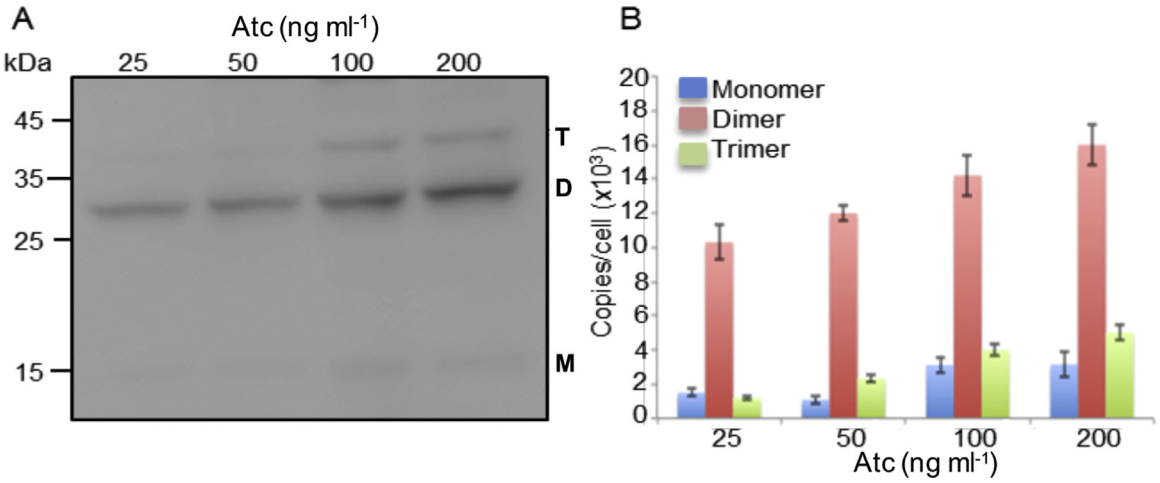

Fig. 9. Ectopic expression of WhiB4. (A) *whiB4-OE* harboring FLAG-tagged WhiB4 under Atc inducible promoter was cultured till OD_{600}nm of 0.4. Expression of WhiB4 was induced by addition of indicated concentration of Atc for 16 h. Approximately, 30 μg of cell free extract from *whiB4-OE* strain was analyzed for WhiB4 expression by immuno-blotting using the antibody against FLAG tag. To minimize the possibility of O_2-induced thiol oxidation and subsequent oligomerization of apo-WhiB4 during cell-free extract preparation, cells were pre-treated with the thiol-alkylating agent NEM as described [20]. Immuno-blot clearly revealed the appearance of monomer (M), dimers (D), and trimers (T) of WhiB4. **(B)** The band intensities were quantified by ImageJ software. Amount of WhiB4 expressed at a single cell level was quantified and plotted as described in Fig. 3.

for WhiB4 and *E. coli* HU, whereas distributions were noticeably skewed towards right in case of CRP (Fig. 14A). Consistent with this, the input normalized signal for peaks identified by the software Model-based Analysis of ChIP-Seq (MACS) for WhiB4 is significantly weaker than peaks identified for *Mtb* CRP (p value $< 10^{-10}$), and comparable to those for *E. coli* HU (Fig. 14B). These observations can be clearly visualized in the UCSC genome browser view showing near-uniform binding of WhiB4 and HU across the genome as opposed to specific-regions of strong binding for CRP (*see* later [Fig. 15]). Finally, ChIP experiments for WhiB4 were consistently successful and obtained high concentrations of DNA (8.54 ng μl^{-1} and 8.52 ng μl^{-1}) as compared to mock-IP (2.72 ng $\mu l^{-1}$and 3.12 ng μl^{-1}) or the strain overexpressing non-DNA binding FLAG-tagged WhiB4-Cys3 variant (3.31 ng $\mu l^{-1}$and 2.98 ng μl^{-1}). Altogether, the data support a more uniform binding of WhiB4 to the chromosome of *Mtb*.

Since above results indicate the presence of weak specificity of WhiB4 to some loci across the *Mtb* genome, we identified these loci by performing peak identification using MACS. This analysis revealed that WhiB4 occupancy positively correlates with the G+C content of the bound DNA (Fig. 14C), which is in agreement with our earlier work on *in vitro* specificity of WhiB4 interaction with the *ahpCD* locus [20]. As expected, a highly GC-rich motif was identified by MEME within these WhiB4 binding peaks (Fig. 14D, E-value: - 6.4 × 10^{-103}). For two independent WhiB4 samples, approximately 700 regions of enriched signals with a remarkable (> 90%) overlap between the binding regions were obtained (Supplementary information Table S4). Approximately, 7–10% of the *Mtb* genome encodes PE and PPE proteins (58, 59). Of the 90 PE proteins, 63 were encoded by GC-rich genes belonging to the PE-PGRS sub-class. Expectedly, WhiB4 bound overwhelmingly to PE-PGRS genes (55 of 63), but marginal to PE/PPE genes that do not belong to the PGRS sub-class (Fig. 15). We confirmed that detection of peaks at the PE-PGRS loci is not an artifact of ambiguous read mapping due to repeat elements present in the PGRS regions. Our peak calling analysis using only reads that can be unequivocally aligned to a single locus on the genome also recovers peaks at the PE-PGRS genes. This result is consistent with the observed preference of WhiB4 for GC rich regions (Fig. 15 and Supplementary information Table S4) and WhiB4-mediated regulation of PE-PGRS expression in *Mycobacterium marinum* [69]. Additionally, genes involved in respiration (*e.g., cydAB*), redox homeostasis (*mshA/B/D, trxB2, nadA/B/C*), and Fe/Fe-S hemostasis (*sufR, sufB, bfrB, mbtB*) were also bound by WhiB4 (Supplementary information Table S4). Interestingly, WhiB4 binds to regions encoding several transcription factors, sigma factors, and NAPs (*lsr2, espR, IHF*) (Supplementary information Table S4). To validate WhiB4 binding, we performed ChIP followed by quantitative PCR (ChIP-qPCR) on 9 target DNA sequences (5 within intergenic regions, 3 within ORFs and 1 non-peak region). Consistent with the ChIP data, all of the selected WhiB4-binding regions showed enrichment (Supplementary information Table S5). As a negative control, we over-expressed the FLAG-tagged WhiB4-Cys3 variant and performed ChIP-qPCR of the WhiB4 targets on immuno-precipitated genomic DNA as described earlier. ChIP-qPCR of WhiB4-specific regions showed no enrichment in the case of WhiB4-Cys3 as compared to corresponding input control (Supplementary information Table S5). Thus, the results indicated that all peaks were likely to be genuine WhiB4-targets.

Finally, we investigated whether genes bound by WhiB4 showed differential expression in *Mtb* during CHP stress. By comparing microarray of CHP-treated wt *Mtb* with the ChIP-seq data, we found that expression was marginally lower for genes bound by WhiB4 than those that are not (p value $< 2.2 \times 10^{-16}$; Supplementary information Fig. S9 and Table S4). Next, we compared ChIP-seq data with the microarray data for CHP-treated *MtbΔwhiB4* (over CHP-treated *Mtb*). Approximately 30% of genes differentially expressed in CHP-treated *MtbΔwhiB4* were bound by WhiB4, indicating both a direct and an indirect influence of WhiB4 on gene expression (Supplementary information Fig. S9 and Table S4). Similar to our findings, studies on FIS and CRP in *E. coli* have found little association between FIS/CRP DNA binding and differential gene expression in Δ*fis*/Δ*crp* strains [70,38]. It was proposed that the primary function of *E. coli* CRP and FIS proteins is to sculpt the chromosome, while their role in regulating transcription is likely to be circumstantial [70,38]. A similar explanation may be suited for WhiB4 as well.

4. Discussion

In this study, we identified a link between DNA condensation, WhiB4, and oxidative stress response in *Mtb*. WhiB proteins are proposed to be Fe-S cluster-containing transcription factors; however, the exact molecular mechanism of action remained poorly understood. Studies revealed that some of the WhiB family members might regulate gene expression by binding to promoter sequences [71,20,27]. Furthermore, ChIP-Seq analysis of WhiB in *Streptomyces coelicolor* (*Sco*)

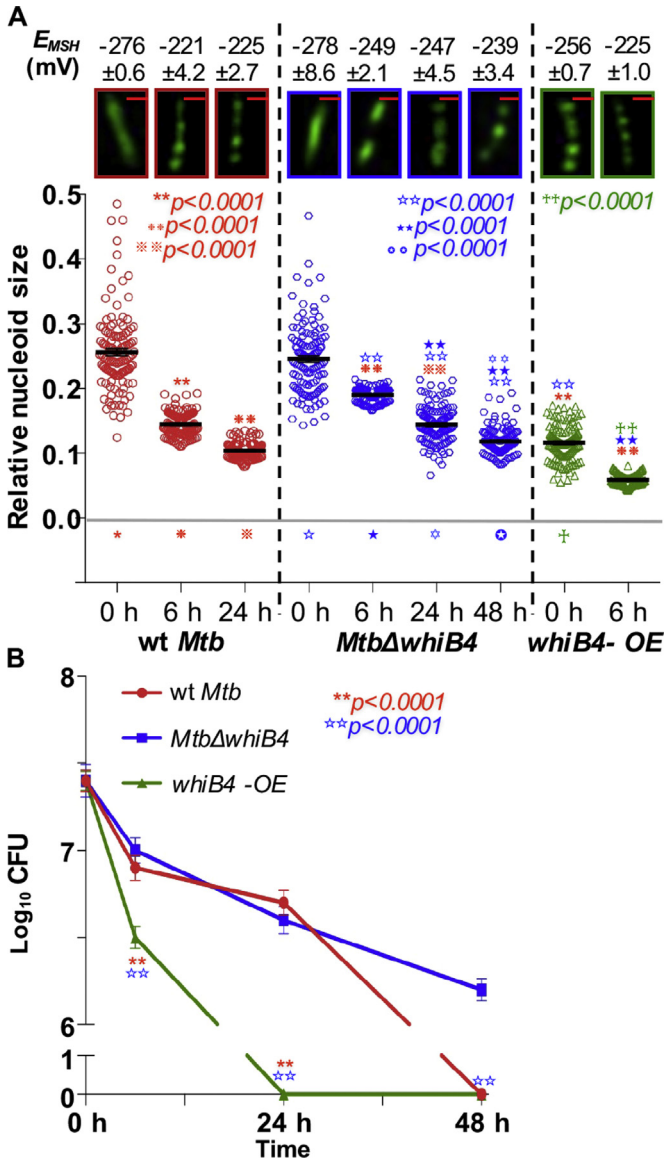

Fig. 10. Oxidative stress leads to DNA condensation, skewed redox homeostasis and bacterial killing in a WhiB4-dependent manner. (A) wt *Mtb, MtbΔwhiB4* and *whiB4-OE* were exposed to 0.5 mM CHP for 6, 24 and 48 h. Nucleoids were stained with DAPI (pseudo colored green) and visualized by confocal microscopy (63X). The scale of images is 1 μm. For inducing WhiB4, 100 ng ml^{-1} of Atc was added to cultures of *whiB4-OE*. As a control, the same amount of Atc was added to other strains. The relative RNS of ~ 100-150 independent cells was measured and represented as scatter plots. Intramycobacterial E_{MSH} of various *Mtb* strains at each time point was measured using flow cytometer and shown along with a corresponding image of a representative DAPI stained cell visualized by confocal microscopy under similar conditions. Data are represented as mean ± SEM. One-way ANOVA with Bonferroni's post hoc test was employed to compare RNS at different time points between all the strains. Comparisons whose p value is < 0.05 were indicated with different symbols. Symbols: (✱): comparison to wt *Mtb* 0 h; (✲): comparison to wt *Mtb* 6 h; (※): comparison to wt *Mtb* 24 h; (☆): comparison to *MtbΔwhiB4* 0 h; (★): comparison to *MtbΔwhiB4* 6 h; (✡): comparison to *MtbΔwhiB4* 24 h; (✪): comparison to *MtbΔwhiB4* 48 h; (□): comparison to *whiB4-OE* 0 h. **(B)** Plots showing the survival of *Mtb* strains in response to CHP stress as assessed by enumerating CFUs (n = 3). Error bars represent mean ± SD. Symbols indicate significant differences using two-way ANOVA with Bonferroni's post hoc test between strains at different time interval as indicated. Symbols: (✱): comparison to wt *Mtb*; (☆): comparison to *MtbΔwhiB4*.

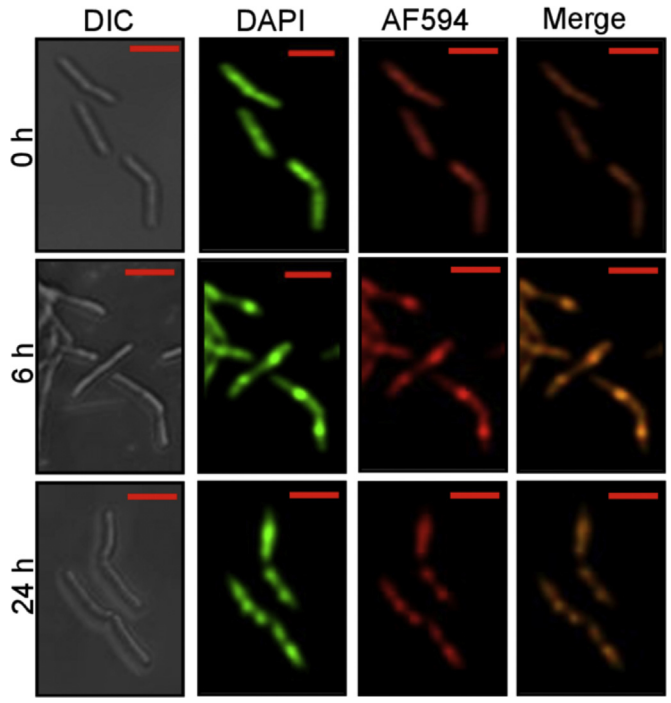

Fig. 11. WhiB4 associates with condensed nucleoid upon oxidative stress. Confocal microscopic images (63X) of *MtbΔwhiB4* cells expressing histidine-tagged WhiB4 (His-WhiB4) from native promoter. The intramycobacterial E_{MSH} of *MtbΔwhiB4* was shifted towards oxidative using 0.5 mM of CHP and WhiB4 association with nucleoids was visualized at various time points post-treatment. Nucleoids were stained with DAPI (pseudo colored green), WhiB4 was marked using anti-His primary antibody and AF594 conjugated secondary antibody (red), and yellow merge indicated co-localization of WhiB4 with DAPI stained nucleoids. The scale bar is 2 μm.

seems to indicate DNA binding wherein a specific regulatory effect may be achieved by its association with a transcription factor WhiA [72]. Here, we confirmed that WhiB4 condenses DNA by binding more uniformly to the *Mtb* chromosome, with a notable preference for GC-rich DNA. Over-expression of WhiB4 induced hyper condensation of nucleoids *in vivo*, indicating that the protein, in sufficient quantity, can function independently in regulating DNA compaction. Notably, over-expression of NAPs (*e.g.* Dps) does not always result in nucleoid condensation owing to the negative influence of other NAPs (*e.g.* Fis) [43]. While overexpression of WhiB4 can condense nucleoid *in vivo*, how it contributes to DNA condensation in conjunction with other mycobacterial NAPs remains to be determined. Moreover, a large majority of WhiB4-binding events are inconsequential from the transcriptional perspective, suggesting that WhiB4-binding does not necessarily affect transcription locally, but may serve as focal points to organize the genome into domains and thereby influence transcription indirectly. In line with this, a genome-wide DNA binding study suggested that ~ 30% of *Mtb* transcription factors binds DNA with a much smaller impact on transcription [73]. Association of WhiB4 with genomic regions encoding Lsr2, EspR, and IHF suggest the possibility of an interplay between different NAPs to alter chromosome structure and organization, thereby influencing patterns of gene expression in response to oxidative stress. Consistent with this, CHP-treated *MtbΔwhiB4* displayed nucleoid compaction (albiet slower), indicating that WhiB4 may collaborate with other NAPs (*e.g.,* Lsr2, EspR, and IHF) under oxidatively hostile conditions.

Several NAPs are known to play important role in influencing nucleoid condensation under specific stress conditions such as iron starvation, hypoxia, and acidic pH [10]. However, the importance of DNA condensation and NAPs in controlling oxidative stress response remains controversial. For example, while *S. aureus* resists H_2O_2 by rapidly

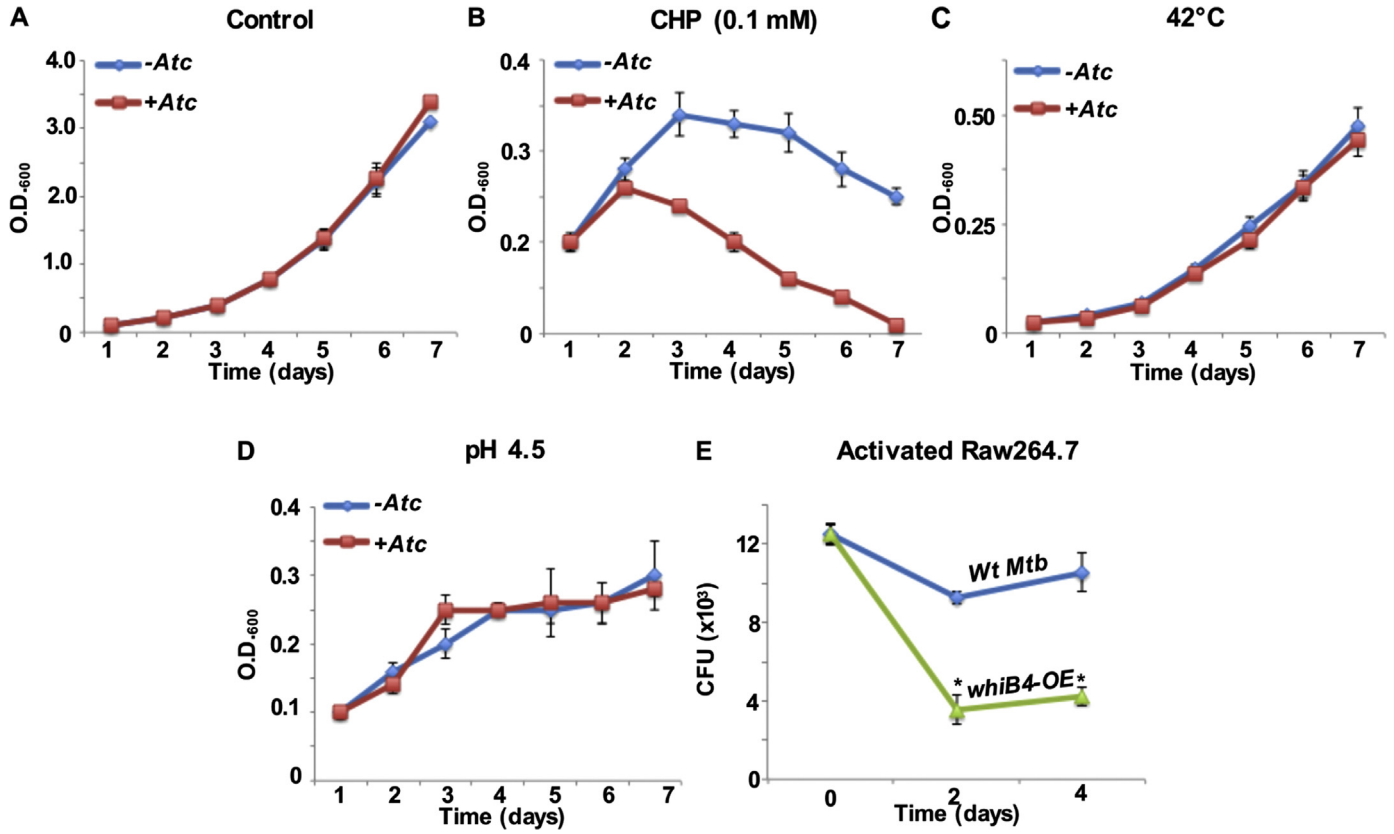

Fig. 12. WhiB4 overexpression specifically reverses phenotypes displayed by *Mtb*Δ*whiB4*. We have earlier shown that *Mtb*Δ*whiB4* survived better upon oxidative stress *in vitro*, inside immune-activated macrophages, and displayed hypervirulence in animals [20]. To investigate the functional relevance of WhiB4 overexpression, we determined the phenotype of WhiB4-OE under defined conditions specific to the WhiB4 function. The *whiB4-OE* strain was either subjected to 200 ng ml^{-1} of Atc induction or left uninduced. Cells were monitored for growth at different time intervals by measuring absorbance at 600 nm under **(A)** aerobic conditions, **(B)** 0.1 mM CHP, **(C)** 42ºC, and **(D)** pH 4.5. Data shown is the average of two experiments performed in triplicates. Error bars represent SD from the mean. **(E)** IFN-ɣ-LPS activated RAW 264.7 macrophages were infected with wt *Mtb*, and *whiB4-OE* strains at an MOI of 10 and survival was monitored by enumerating CFU. Infected macrophages were maintained in 200 ng ml^{-1} of Atc for sustained induction of WhiB4. The data is shown as Mean ± SD from two independent experiments having triplicate wells each. Two tailed Student's *t*-test was used to determine statistical significance and is indicated where differences were significant *P < 0.05.

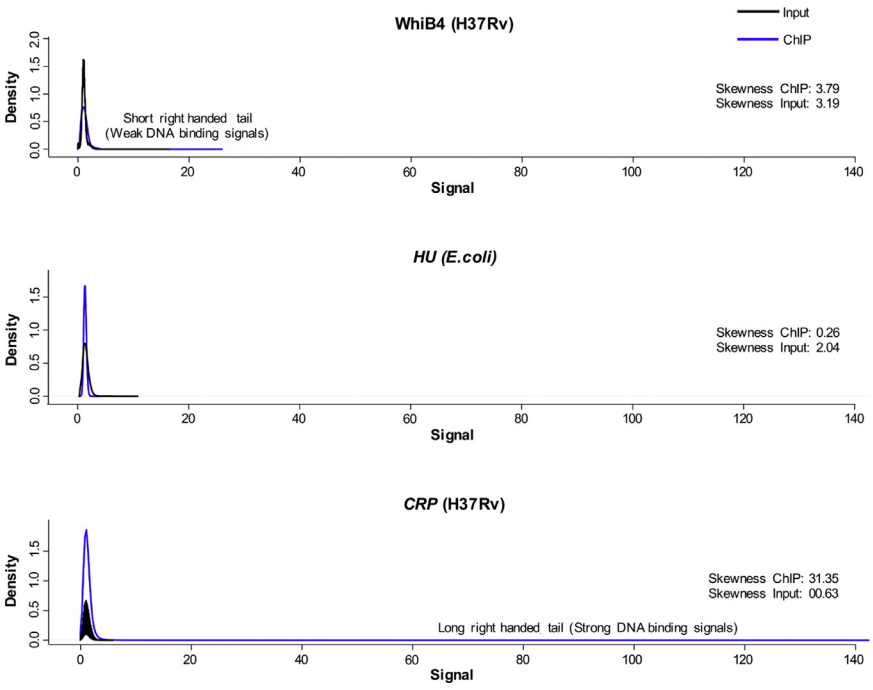

Fig. 13. Density distribution plots for the Z-score distribution for *Mtb* WhiB4, *E.coli* HU and *Mtb* CRP. ChIP signal is shown in blue and the input signal is shown in black. Compared to CRP ChIP, the distribution of the WhiB4 and *E. coli* HU distribution does not have the characteristic heavy right end tail. This is also evident from the skewness measured for each distribution. Positive skewness values depict right-handed distribution as in the case of CRP ChIP and slightly in the WhiB4 ChIP.

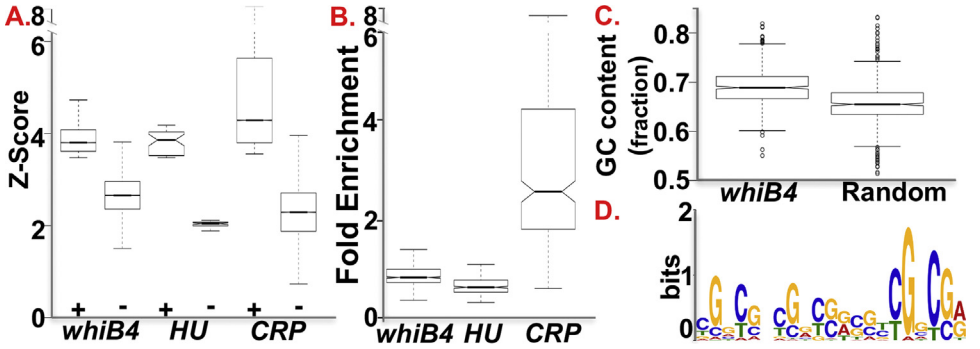

Fig. 14. WhiB4 exhibits largely uniform binding to the *Mtb* chromosome. The left panel shows **(A)** boxplots displaying the distribution above the threshold Z-score (Z-score > 3) in the right-hand tail region (enriched DNA binding) for ChIP samples and the corresponding Z-score values in the input for WhiB4 replicate 1, HU and CRP. The difference between the ChIP enriched regions is significant against the input control in the case of CRP, a specific binding transcription factor (Wilcoxon test, $P < 10^{-10}$) as well as WhiB4 and HU (Wilcoxon test, $P < 10^{-10}$), **(B)** Fold enrichment distribution as observed for WhiB4, HU and CRP using MACS peak calling. On the y-axis is the fold enrichment denoted for each peak identified in the analyses. WhiB4 fold enrichment is less and similar to HU, whereas CRP shows higher values for fold enrichment in its peaks. **(C)** Boxplot showing GC content distribution between the obtained peaks for WhiB4 *versus* randomized peaks from the *Mtb* H37Rv genome. The WhiB4 peaks in comparison with the randomized input regions have higher GC content (Wilcoxon test, $P < 10^{-10}$). **(D)** GC-rich motif obtained from the WhiB4 peaks using MEME-ChIP suite (web interface).

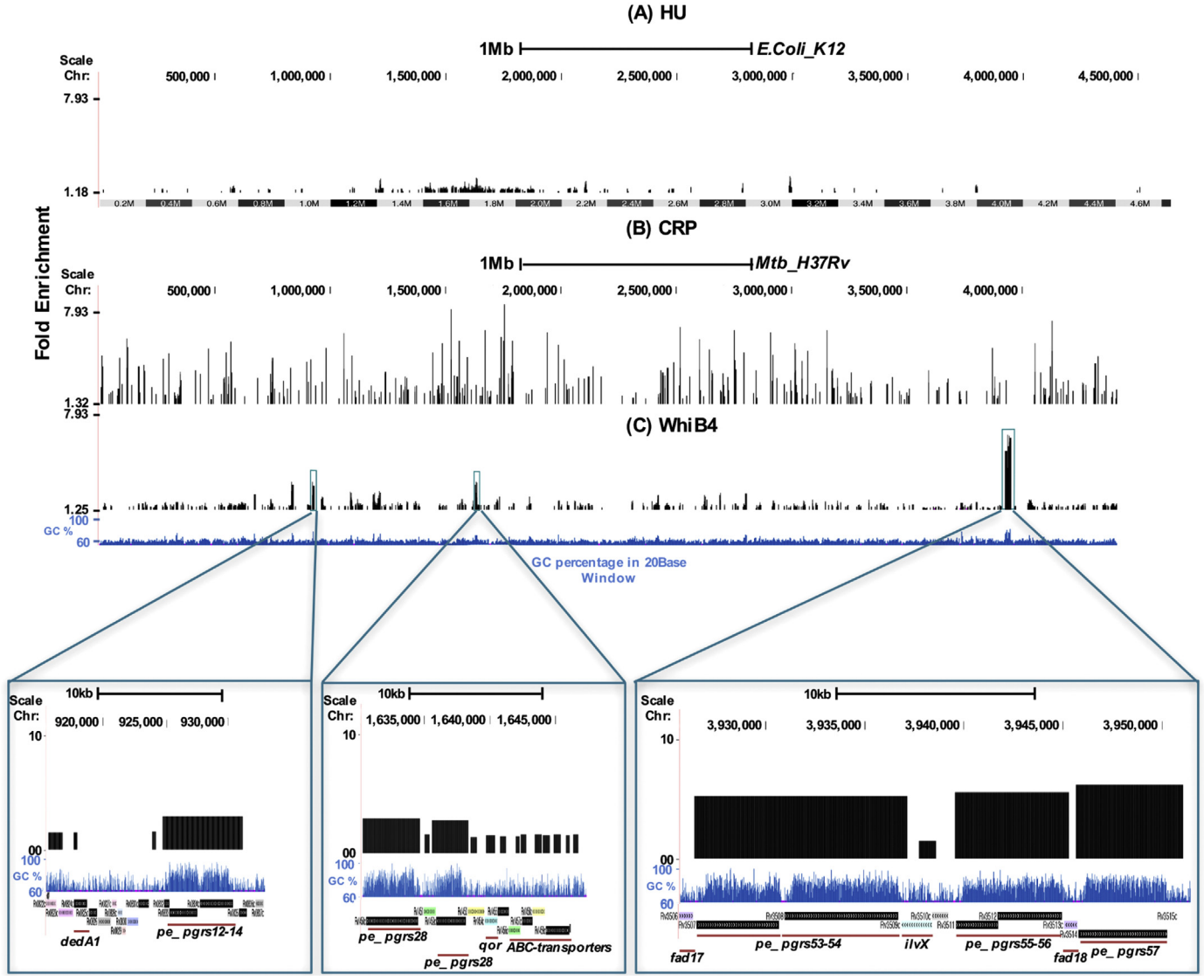

Fig. 15. Genome wide mapping of WhiB4 binding sites. Input normalized HU, CRP, and WhiB4 binding on the respective chromosome as visualized on the UCSC genome browser with the corresponding GC% for WhiB4 and CRP. On the y-axis is the fold enrichment of the peaks. WhiB4 peaks in majority of the cases are observed in the genomic regions rich in GC content as seen in the zoomed in examples.

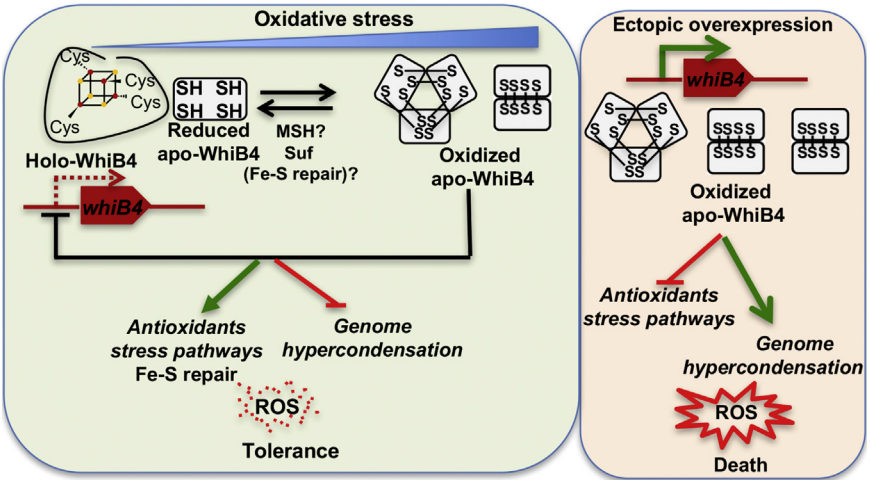

Fig. 16. Proposed model of WhiB4 function in oxidative stress response. Under mild oxidative conditions, a minor fraction of oxidized apo-WhiB4 generated *via* oxidation of holo-WhiB4 activates DNA binding and repressor function to preclude unnecessary overexpression of oxidative stress responsive pathways. Further elevation in oxidative stress levels result in higher thiol-linked apo-WhiB4 oligomers, which would have further repressed antioxidants expression and induced genome hypercondensation. To circumvent this, *Mtb* downregulates expression of WhiB4 (*via* autorepression) to control the levels of oxidized apo-WhiB4, which ensures appropriated degree of nucleoid condensation and antioxidants expression. A gradual increase in antioxidants such as MSH and the Fe-S repair pathways (Suf operon) can create a regulatory feedback loop, which reduces oxidized thiols of apo-WhiB4 to eventually regenerate monomeric reduced apo-WhiB4/holo-WhiB4. All of this ultimately results in complete derepression of antioxidants to mitigate oxidative stress and to also restore topological homeostasis. Ectopic over-expression of WhiB4 by Atc leads to sustained accumulation of oxidized apo-WhiB4 without any feedback control. This eventually represses antioxidants/stress pathways and induces long lasting nucleoid hypercondensation. Both of these activities of WhiB4 adversely affect mycobacterial ability to tolerate oxidative stress leading to enhanced susceptibility of *whiB4-OE* strain towards CHP.

condensing DNA through a Dps homolog (MrgA) [13], oxidative stress simply did not lead to DNA condensation in other bacteria including *Sco*, *Dickeya dadantii*, and *E. coli* [74,43,75]. Interestingly, a recent study elegantly showed that MrgA-mediated protection of *S. aureus* from oxidative stress is mainly due to its ferroxidase activity rather than its ability to shield DNA [76]. However, the role of Lsr2 in protecting *Mtb* from oxidative damage by shielding DNA is controversial [11,77]. Therefore, it is unclear as of now how mycobacteria remodel their DNA condensation during oxidative stress. To begin understanding this, we demonstrated that the loss of WhiB4 delays DNA condensation, maintains redox homeostasis, and protects the cells from oxidative stress, whereas its over-expression reversed these phenotypes. Our data indicate that the detrimental effect of WhiB4 overexpression is likely to be due to the repression of antioxidant machinery and the diminished capacity to counteract cytoplasmic redox stress. It is also likely that hyper-condensation of the nucleoid inhibits other metabolic processes such as DNA replication/repair, transcription, and translation to exert efficient killing. We conclude that resistance to oxidative stress in *Mtb* is unlikely to be mediated by nucleoid hypercompaction. In this context, it has been suggested that certain bacteria (*e.g.,* gamma-proteobacteria) have evolved genetic mechanisms (*e.g.* Fis, TopA, and GyrA) to block DNA condensation and promote the expression of OxyR-dependent antioxidant genes as a major mechanism to guard genomic DNA against oxidative stress [43]. Moreover, similar to *Mtb*, a higher degree of oxidative stress and killing were associated with nucleoid hypercondensation in *E. coli* [78,16]. Although, unlike *Mtb* where WhiB4 overexpression is sufficient to induce both DNA condensation and killing under oxidative stress, a similar consequence of oxidative challenge seems to be mediated through a combined action of multiple OxyR-regulated NAPs (*e.g*, H-NS, Hup, Him, MukB, and Dps) in *E.coli* [16]. In the absence of OxyR, Fis and Dps activities in *Mtb*, WhiB4, with its redox-active cysteines can be an important regulator of both nucleoid condensation and expression of oxidative stress responsive genes in *Mtb*.

We have previously shown that the 4Fe−4S cluster of WhiB4 is exceptionally sensitive to oxygen *in vitro* [20]. Consistent with this, we showed the presence of a minor fraction of disulfide-linked apo-WhiB4 oligomer under aerobic growing condition. This indicates that despite the reduced environment of mycobacterial cytosol, WhiB4 Fe-S cluster can be targeted during aerobic metabolism to generate apo-WhiB4. Since Fe-S clusters are acutely sensitive to superoxide generated during aerobic respiration [79], it is likely that WhiB4 Fe-S cluster is oxidatively damaged by superoxide during aerobic growth. However, this requires future experimentation. Further oxidation of WhiB4 thiols would require two-electron oxidation by free radicals as triggered upon exposure to CHP. This form of oxidized apo-WhiB4 oligomer is involved in nucleoid condensation and gene expression in *Mtb*. Interestingly, the four redox-active cysteine (Cys) residues involved in Fe-S cluster coordination in WhiB4 are surrounded by several basic amino acids (Lys36–Cys37–Arg38, Cys59–Arg60), which may decrease Cys residues pKa, resulting in the formation of disulfide bonds in the cytosol of mycobacteria. We propose that under aerobic growing conditions, oxidation of holo-WhiB4 to oxidized apo-WhiB4 activates DNA binding and repressor function to preclude the unnecessary expression of oxidative stress responsive pathways. A gradual increase in oxidative stress on the one hand increases generation of oxidized apo-WhiB4 oligomers while on the other hand down-regulates WhiB4 expression. Both of these activities ensure levels of intracellular oxidized apo-WhiB4 oligomers required to induce appropriate degree of nucleoid condensation and calibrated activation of antioxidants/stress pathways. The steady increase in antioxidants such as MSH and Fe-S biogenesis machinery (Suf operon) in response to sustained oxidative stress can create a regulatory feedback loop by reducing oxidized thiols of apo-WhiB4 to regenerate monomeric reduced apo-WhiB4 and/or holo-WhiB4. This would allow WhiB4 to loose chromosomal binding and completely derepress antioxidants, maintaining both redox and topological balance (Fig. 16). Besides this, other factors (*e.g.,* NAPs, sigma factors *etc.*) which directly or indirectly cooperate with WhiB4 could play a role in maintaining topological homeostasis and adaptation to oxidative stress. The fact that *Mtb*Δ*whiB4* showed higher resistance to oxidative stress and *whiB4-OE* displayed hypersensitivity as compared to wt *Mtb* indicates that a gradual decrease in WhiB4 expression upon oxidative stress is a cellular decision to induce the oxidative stress response and reduce DNA hypercondensation.

5. Conclusion

In conclusion, the combined results indicate that WhiB4 is a candidate for a dual-function NAP that could integrate environmental signals with DNA conformation and transcription. The focus of the present investigations has been mainly on the nucleoid condensing function of WhiB4 and how it can modulate oxidative stress response in *Mtb*. As far as we are aware, this is the first example of a redox-dependent NAP in bacteria.

Acknowledgements

We are thankful to the University of Delhi South Campus MicroArray Centre (UDSCMAC), New Delhi, for conducting the microarray experiments. We thank IISc and ICGEB for providing BSL3 facilities. We are grateful to the Imaging facilities at University of Delhi, South Campus, New Delhi, and IISc, Bangalore. We thank Monisha Mohandas (AFM facility, BSSE, IISc Bangalore) for excellent technical help. The *Mtb* work was supported by the following Wellcome Trust/DBT India Alliance Grants, WT-DBT/500034-Z-09-Z (AS), IA/S/16/2/502700 (AS), IA/E/16/1/503017 (KA), and in part by Department of Biotechnology (DBT) Grant BT/PR11911/BRB/10/1327/2014, BT/PR5020/MED/29/1454/2012 (AS) and DBT-IISc Partnership Program (22-0905-0006-05-987-436). AS and KA are senior- and early- career fellows of Wellcome Trust/DBT India Alliance.

Author contributions

MC, SM, KA, PP and AS participated in the design of the study; MC, SM, KA, PP, MM, TV,PS, KJ, HNV, PA, MG, ASNV, and AS carried out the experiments and the data analysis. MC, SM, KA and AS conceived the study, supervised the project, and drafted the manuscript. All authors read and approved the final manuscript.

Conflict of interest statement

The authors have no conflict of interests to declare.

Appendix A. Supplementary material

Supplementary data associated with this article can be found in the online version at doi:10.1016/j.redox.2018.08.006.

References

[1] S. Ehrt, D. Schnappinger, Mycobacterial survival strategies in the phagosome: defence against host stresses, Cell Microbiol. 11 (2009) 1170–1178.
[2] K. Sato, T. Akaki, H. Tomioka, Differential potentiation of anti-mycobacterial activity and reactive nitrogen intermediate-producing ability of murine peritoneal macrophages activated by interferon-gamma (IFN-gamma) and tumour necrosis factor-alpha (TNF-alpha), Clin. Exp. Immunol. 112 (1998) 63–68.
[3] M.R. Hasan, M. Rahman, S. Jaques, E. Purwantini, L. Daniels, Glucose 6-phosphate accumulation in mycobacteria: implications for a novel F420-dependent anti-oxidant defense system, J. Biol. Chem. 285 (2010) 19135–19144.
[4] A. Koshkin, X.T. Zhou, C.N. Kraus, J.M. Brenner, P. Bandyopadhyay, I.D. Kuntz, C.E. Barry 3rd, P.R. Ortiz de Montellano, Inhibition of *Mycobacterium tuberculosis* AhpD, an element of the peroxiredoxin defense against oxidative stress, Antimicrob. Agents Chemother. 48 (2004) 2424–2430.
[5] K. Lin, K.M. O'Brien, C. Trujillo, R. Wang, J.B. Wallach, D. Schnappinger, S. Ehrt, *Mycobacterium tuberculosis* thioredoxin reductase is essential for thiol redox homeostasis but plays a minor role in antioxidant defense, PLoS Pathog. 12 (2016) e1005675.
[6] C. Manca, S. Paul, C.E. Barry 3rd, V.H. Freedman, G. Kaplan, *Mycobacterium tuberculosis* catalase and peroxidase activities and resistance to oxidative killing in human monocytes in vitro, Infect. Immun. 67 (1999) 74–79.
[7] S. Nambi, J.E. Long, B.B. Mishra, R. Baker, K.C. Murphy, A.J. Olive, H.P. Nguyen, S.A. Shaffer, C.M. Sassetti, The oxidative stress network of *Mycobacterium tuberculosis* reveals coordination between radical detoxification systems, Cell Host Microbe 17 (2015) 829–837.
[8] D.L. Piddington, F.C. Fang, T. Laessig, A.M. Cooper, I.M. Orme, N.A. Buchmeier, Cu,Zn superoxide dismutase of *Mycobacterium tuberculosis* contributes to survival in activated macrophages that are generating an oxidative burst, Infect. Immun. 69 (2001) 4980–4987.
[9] D.R. Sherman, P.J. Sabo, M.J. Hickey, T.M. Arain, G.G. Mahairas, Y. Yuan, C.E. Barry 3rd, C.K. Stover, Disparate responses to oxidative stress in saprophytic and pathogenic mycobacteria, Proc. Natl. Acad. Sci. USA 92 (1995) 6625–6629.
[10] S.C. Dillon, C.J. Dorman, Bacterial nucleoid-associated proteins, nucleoid structure and gene expression, Nat. Rev. Microbiol 8 (2010) 185–195.
[11] R. Colangeli, A. Haq, V.L. Arcus, E. Summers, R.S. Magliozzo, A. McBride, A.K. Mitra, M. Radjainia, A. Khajo, W.R. Jacobs Jr., P. Salgame, D. Alland, The multifunctional histone-like protein Lsr2 protects mycobacteria against reactive oxygen intermediates, Proc. Natl. Acad. Sci. USA 106 (2009) 4414–4418.
[12] A. Martinez, R. Kolter, Protection of DNA during oxidative stress by the nonspecific DNA-binding protein Dps, J. Bacteriol. 179 (1997) 5188–5194.
[13] K. Morikawa, R.L. Ohniwa, J. Kim, A. Maruyama, T. Ohta, K. Takeyasu, Bacterial nucleoid dynamics: oxidative stress response in Staphylococcus aureus, Genes Cells 11 (2006) 409–423.
[14] H. Wang, F. Wang, X. Hua, T. Ma, J. Chen, X. Xu, L. Wang, B. Tian, Y. Hua, Genetic and biochemical characteristics of the histone-like protein DR0199 in *Deinococcus radiodurans*, Microbiology 158 (2012) 936–943.
[15] D. Weinstein-Fischer, M. Elgrably-Weiss, S. Altuvia, *Escherichia coli* response to hydrogen peroxide: a role for DNA supercoiling, topoisomerase I and Fis, Mol. Microbiol. 35 (2000) 1413–1420.
[16] K.C. Ko, P.C. Tai, C.D. Derby, Mechanisms of action of escapin, a bactericidal agent in the ink secretion of the sea hare Aplysia californica: rapid and long-lasting DNA condensation and involvement of the OxyR-regulated oxidative stress pathway, Antimicrob. Agents Chemother. 56 (2012) 1725–1734.
[17] T. Bhowmick, S. Ghosh, K. Dixit, V. Ganesan, U.A. Ramagopal, D. Dey, S.P. Sarma, S. Ramakumar, V. Nagaraja, Targeting *Mycobacterium tuberculosis* nucleoid-associated protein HU with structure-based inhibitors, Nat. Commun. 5 (2014) 4124.
[18] B. Blasco, J.M. Chen, R. Hartkoorn, C. Sala, S. Uplekar, J. Rougemont, F. Pojer, S.T. Cole, Virulence regulator EspR of *Mycobacterium tuberculosis* is a nucleoid-associated protein, PLoS Pathog. 8 (2012) e1002621.
[19] S. Casonato, A. Cervantes Sanchez, H. Haruki, M. Rengifo Gonzalez, R. Provvedi, E. Dainese, T. Jaouen, S. Gola, E. Bini, M. Vicente, K. Johnsson, D. Ghisotti, G. Palu, R. Hernandez-Pando, R. Manganelli, WhiB5, a transcriptional regulator that contributes to *Mycobacterium tuberculosis* virulence and reactivation, Infect. Immun. 80 (2012) 3132–3144.
[20] M. Chawla, P. Parikh, A. Saxena, M. Munshi, M. Mehta, D. Mai, A.K. Srivastava, K.V. Narasimhulu, K.E. Redding, N. Vashi, D. Kumar, A.J. Steyn, A. Singh, *Mycobacterium tuberculosis* WhiB4 regulates oxidative stress response to modulate survival and dissemination in vivo, Mol. Microbiol. 85 (2012) 1148–1165.
[21] Z. Chen, Y. Hu, B.M. Cumming, P. Lu, L. Feng, J. Deng, A.J. Steyn, S. Chen, Mycobacterial WhiB6 differentially regulates ESX-1 and the Dos Regulon to modulate granuloma formation and virulence in zebrafish, Cell Rep. 16 (2016) 2512–2524.
[22] M. Konar, M.S. Alam, C. Arora, P. Agrawal, WhiB2/Rv3260c, a cell division-associated protein of *Mycobacterium tuberculosis* H37Rv, has properties of a chaperone, FEBS J. 279 (2012) 2781–2792.
[23] M. Mehta, R.S. Rajmani, A. Singh, *Mycobacterium tuberculosis* WhiB3 responds to vacuolar pH-induced changes in mycothiol redox potential to modulate phagosomal maturation and virulence, J. Biol. Chem. 291 (2016) 2888–2903.
[24] S. Mishra, P. Shukla, A. Bhaskar, K. Anand, P. Baloni, R.K. Jha, A. Mohan, R.S. Rajmani, V. Nagaraja, N. Chandra, A. Singh, Efficacy of beta-lactam/beta-lactamase inhibitor combination is linked to WhiB4-mediated changes in redox physiology of *Mycobacterium tuberculosis*, Elife 6 (2017).
[25] R.P. Morris, L. Nguyen, J. Gatfield, K. Visconti, K. Nguyen, D. Schnappinger, S. Ehrt, Y. Liu, L. Heifets, J. Pieters, G. Schoolnik, C.J. Thompson, Ancestral antibiotic resistance in *Mycobacterium tuberculosis*, Proc. Natl. Acad. Sci. USA 102 (2005) 12200–12205.
[26] T.R. Raghunand, W.R. Bishai, *Mycobacterium smegmatis* whmD and its homologue Mycobacterium tuberculosis whiB2 are functionally equivalent, Microbiology 152 (2006) 2735–2747.
[27] A. Singh, D.K. Crossman, D. Mai, L. Guidry, M.I. Voskuil, M.B. Renfrow, A.J. Steyn, *Mycobacterium tuberculosis* WhiB3 maintains redox homeostasis by regulating virulence lipid anabolism to modulate macrophage response, PLoS Pathog. 5 (2009) e1000545.
[28] A. Singh, L. Guidry, K.V. Narasimhulu, D. Mai, J. Trombley, K.E. Redding, G.I. Giles, J.R. Lancaster Jr., A.J. Steyn, *Mycobacterium tuberculosis* WhiB3 responds to O2 and nitric oxide via its [4Fe-4S] cluster and is essential for nutrient starvation survival, Proc. Natl. Acad. Sci. USA 104 (2007) 11562–11567.
[29] L.J. Smith, M.R. Stapleton, G.J. Fullstone, J.C. Crack, A.J. Thomson, N.E. Le Brun, D.M. Hunt, E. Harvey, S. Adinolfi, R.S. Buxton, J. Green, *Mycobacterium tuberculosis* WhiB1 is an essential DNA-binding protein with a nitric oxide-sensitive iron-sulfur cluster, Biochem J. 432 (2010) 417–427.
[30] J. Rybniker, A. Nowag, E. van Gumpel, N. Nissen, N. Robinson, G. Plum, P. Hartmann, Insights into the function of the WhiB-like protein of mycobacteriophage TM4–a transcriptional inhibitor of WhiB2, Mol. Microbiol. 77 (2010) 642–657.
[31] B. Venkataraman, M. Vasudevan, A. Gupta, A new microarray platform for whole-genome expression profiling of *Mycobacterium tuberculosis*, J. Microbiol. Methods 97 (2014) 34–43.
[32] H. Li, R. Durbin, Fast and accurate short read alignment with Burrows-Wheeler transform, Bioinformatics 25 (2009) 1754–1760.
[33] H. Li, B. Handsaker, A. Wysoker, T. Fennell, J. Ruan, N. Homer, G. Marth, G. Abecasis, R. Durbin, S. Genome Project Data Processing, The sequence alignment/map format and SAMtools, Bioinformatics 25 (2009) 2078–2079.
[34] A.R. Quinlan, I.M. Hall, BEDTools: a flexible suite of utilities for comparing genomic features, Bioinformatics 26 (2010) 841–842.
[35] Y. Zhang, T. Liu, C.A. Meyer, J. Eeckhoute, D.S. Johnson, B.E. Bernstein, C. Nusbaum, R.M. Myers, M. Brown, W. Li, X.S. Liu, Model-based analysis of ChIP-Seq (MACS), Genome Biol. 9 (2008) R137.
[36] P.P. Chan, A.D. Holmes, A.M. Smith, D. Tran, T.M. Lowe, The UCSC Archaeal genome browser: 2012 update, Nucleic Acids Res. 40 (2012) D646–D652.
[37] P. Machanick, T.L. Bailey, MEME-ChIP: motif analysis of large DNA datasets, Bioinformatics 27 (2011) 1696–1697.
[38] C. Kahramanoglou, A.S. Seshasayee, A.I. Prieto, D. Ibberson, S. Schmidt, J. Zimmermann, V. Benes, G.M. Fraser, N.M. Luscombe, Direct and indirect effects of H-NS and Fis on global gene expression control in Escherichia coli, Nucleic Acids Res. 39 (2011) 2073–2091.
[39] W. Huber, V.J. Carey, R. Gentleman, S. Anders, M. Carlson, B.S. Carvalho,

H.C. Bravo, S. Davis, L. Gatto, T. Girke, R. Gottardo, F. Hahne, K.D. Hansen, R.A. Irizarry, M. Lawrence, M.I. Love, J. MacDonald, V. Obenchain, A.K. Oles, H. Pages, A. Reyes, P. Shannon, G.K. Smyth, D. Tenenbaum, L. Waldron, M. Morgan, Orchestrating high-throughput genomic analysis with Bioconductor, Nat Methods 12 (2015), pp. 115–121.

[40] A. Takade, K. Takeya, H. Taniguchi, Y. Mizuguchi, Electron microscopic observations of cell division in Mycobacterium vaccae V1, J. Gen. Microbiol. 129 (1983) 2315–2320.

[41] S. Vijay, D. Anand, P. Ajitkumar, Unveiling unusual features of formation of septal partition and constriction in mycobacteria–an ultrastructural study, J. Bacteriol. 194 (2012) 702–707.

[42] A. Bhaskar, M. Chawla, M. Mehta, P. Parikh, P. Chandra, D. Bhave, D. Kumar, K.S. Carroll, A. Singh, Reengineering redox sensitive GFP to measure mycothiol redox potential of *Mycobacterium tuberculosis* during infection, PLoS Pathog. 10 (2014) e1003902.

[43] R.L. Ohniwa, K. Morikawa, J. Kim, T. Ohta, A. Ishihama, C. Wada, K. Takeyasu, Dynamic state of DNA topology is essential for genome condensation in bacteria, EMBO J. 25 (2006) 5591–5602.

[44] R. Schneider, A. Travers, T. Kutateladze, G. Muskhelishvili, A DNA architectural protein couples cellular physiology and DNA topology in Escherichia coli, Mol. Microbiol. 34 (1999) 953–964.

[45] M.I. Voskuil, I.L. Bartek, K. Visconti, G.K. Schoolnik, The response of *Mycobacterium tuberculosis* to reactive oxygen and nitrogen species, Front. Microbiol. 2 (2011) 105.

[46] Y. Hu, A.R. Coates, Acute and persistent *Mycobacterium tuberculosis* infections depend on the thiol peroxidase TpX, PLoS One 4 (2009) e5150.

[47] C. Maksymiuk, A. Balakrishnan, R. Bryk, K.Y. Rhee, C.F. Nathan, E1 of alpha-ketoglutarate dehydrogenase defends *Mycobacterium tuberculosis* against glutamate anaplerosis and nitroxidative stress, Proc. Natl. Acad. Sci. USA 112 (2015) E5834–E5843.

[48] S.S. Master, B. Springer, P. Sander, E.C. Boettger, V. Deretic, G.S. Timmins, Oxidative stress response genes in *Mycobacterium tuberculosis*: role of ahpC in resistance to peroxynitrite and stage-specific survival in macrophages, Microbiology 148 (2002) 3139–3144.

[49] R. Pathania, N.K. Navani, A.M. Gardner, P.R. Gardner, K.L. Dikshit, Nitric oxide scavenging and detoxification by the *Mycobacterium tuberculosis* haemoglobin, HbN in Escherichia coli, Mol. Microbiol. 45 (2002) 1303–1314.

[50] K.S. Ung, Y. Av-Gay, Mycothiol-dependent mycobacterial response to oxidative stress, FEBS Lett. 580 (2006) 2712–2716.

[51] A. Venugopal, R. Bryk, S. Shi, K. Rhee, P. Rath, D. Schnappinger, S. Ehrt, C. Nathan, Virulence of *Mycobacterium tuberculosis* depends on lipoamide dehydrogenase, a member of three multienzyme complexes, Cell Host Microbe 9 (2011) 21–31.

[52] S. Al-Attar, Y. Yu, M. Pinkse, J. Hoeser, T. Friedrich, D. Bald, S. de Vries, Cytochrome bd displays significant quinol peroxidase activity, Sci. Rep. 6 (2016) 27631.

[53] P. Lu, M.H. Heineke, A. Koul, K. Andries, G.M. Cook, H. Lill, R. van Spanning, D. Bald, The cytochrome bd-type quinol oxidase is important for survival of *Mycobacterium smegmatis* under peroxide and antibiotic-induced stress, Sci. Rep. 5 (2015) 10333.

[54] S. Fishbein, N. van Wyk, R.M. Warren, S.L. Sampson, Phylogeny to function: pe/ppe protein evolution and impact on *Mycobacterium tuberculosis* pathogenicity, Mol. Microbiol. 96 (2015) 901–916.

[55] P. Ramakrishnan, A.M. Aagesen, J.D. McKinney, A.D. Tischler, *Mycobacterium tuberculosis* resists stress by regulating PE19 expression, Infect. Immun. 84 (2015) 735–746.

[56] V. Anil Kumar, R. Goyal, R. Bansal, N. Singh, R.R. Sevalkar, A. Kumar, D. Sarkar, EspR-dependent ESAT-6 protein secretion of *Mycobacterium tuberculosis* requires the presence of virulence regulator PhoP, J. Biol. Chem. 291 (2016) 19018–19030.

[57] L. Solans, N. Aguilo, S. Samper, A. Pawlik, W. Frigui, C. Martin, R. Brosch, J. Gonzalo-Asensio, A specific polymorphism in *Mycobacterium tuberculosis* H37Rv causes differential ESAT-6 expression and identifies WhiB6 as a novel ESX-1 component, Infect. Immun. 82 (2014) 3446–3456.

[58] M. Bhattacharya, A.K. Das, Inverted repeats in the promoter as an autoregulatory sequence for TcrX in *Mycobacterium tuberculosis*, Biochem. Biophys. Res. Commun. 415 (2011) 17–23.

[59] R.T. Dame, N. Goosen, HU: promoting or counteracting DNA compaction? FEBS Lett. 529 (2002) 151–156.

[60] I. Tessmer, T. Moore, R.G. Lloyd, A. Wilson, D.A. Erie, S. Allen, S.J. Tendler, AFM studies on the role of the protein RdgC in bacterial DNA recombination, J. Mol. Biol. 350 (2005) 254–262.

[61] J. van Noort, S. Verbrugge, N. Goosen, C. Dekker, R.T. Dame, Dual architectural roles of HU: formation of flexible hinges and rigid filaments, Proc. Natl. Acad. Sci. USA 101 (2004) 6969–6974.

[62] L. Barksdale, K.S. Kim, Mycobacterium, Bacteriol. Rev. 41 (1977) 217–372.

[63] S. Vijay, M. Nagaraja, J. Sebastian, P. Ajitkumar, Asymmetric cell division in *Mycobacterium tuberculosis* and its unique features, Arch. Microbiol. 196 (2014) 157–168.

[64] C. Vilcheze, Y. Av-Gay, R. Attarian, Z. Liu, M.H. Hazbon, R. Colangeli, B. Chen, W. Liu, D. Alland, J.C. Sacchettini, W.R. Jacobs Jr., Mycothiol biosynthesis is essential for ethionamide susceptibility in *Mycobacterium tuberculosis*, Mol. Microbiol. 69 (2008) 1316–1329.

[65] N.A. Buchmeier, G.L. Newton, T. Koledin, R.C. Fahey, Association of mycothiol with protection of M*ycobacterium tuberculosis* from toxic oxidants and antibiotics, Mol. Microbiol 47 (2003) 1723–1732.

[66] J.E. Galagan, K. Minch, M. Peterson, A. Lyubetskaya, E. Azizi, L. Sweet, A. Gomes, T. Rustad, G. Dolganov, I. Glotova, T. Abeel, C. Mahwinney, A.D. Kennedy, R. Allard, W. Brabant, A. Krueger, S. Jaini, B. Honda, W.H. Yu, M.J. Hickey, J. Zucker, C. Garay, B. Weiner, P. Sisk, C. Stolte, J.K. Winkler, Y. Van de Peer, P. Iazzetti, D. Camacho, J. Dreyfuss, Y. Liu, A. Dorhoi, H.J. Mollenkopf, P. Drogaris, J. Lamontagne, Y. Zhou, J. Piquenot, S.T. Park, S. Raman, S.H. Kaufmann, R.P. Mohney, D. Chelsky, D.B. Moody, D.R. Sherman, G.K. Schoolnik, The *Mycobacterium tuberculosis* regulatory network and hypoxia, Nature 499 (2013) 178–183.

[67] C. Kahramanoglou, T. Cortes, N. Matange, D.M. Hunt, S.S. Visweswariah, D.B. Young, R.S. Buxton, Genomic mapping of cAMP receptor protein (CRP Mt) in *Mycobacterium tuberculosis*: relation to transcriptional start sites and the role of CRPMt as a transcription factor, Nucleic Acids Res. 42 (2014) 8320–8329.

[68] A.I. Prieto, C. Kahramanoglou, R.M. Ali, G.M. Fraser, A.S. Seshasayee, N.M. Luscombe, Genomic analysis of DNA binding and gene regulation by homologous nucleoid-associated proteins IHF and HU in *Escherichia coli* K12, Nucleic Acids Res 40 (2012) 3524–3537.

[69] J. Wu, H.W. Ru, Z.H. Xiang, J. Jiang, Y.C. Wang, L. Zhang, J. Liu, WhiB4 regulates the PE/PPE gene family and is essential for virulence of *Mycobacterium marinum*, Sci. Rep. 7 (2017) 3007.

[70] D.C. Grainger, D. Hurd, M. Harrison, J. Holdstock, S.J. Busby, Studies of the distribution of Escherichia coli cAMP-receptor protein and RNA polymerase along the *E. coli* chromosome, Proc. Natl. Acad. Sci. USA 102 (2005) 17693–17698.

[71] J. Burian, S. Ramon-Garcia, C.G. Howes, C.J. Thompson, WhiB7, a transcriptional activator that coordinates physiology with intrinsic drug resistance in *Mycobacterium tuberculosis*, Expert Rev. Anti Infect. Ther. 10 (2012) 1037–1047.

[72] M.J. Bush, G. Chandra, M.J. Bibb, K.C. Findlay, M.J. Buttner, Genome-wide chromatin immunoprecipitation sequencing analysis shows that WhiB is a transcription factor that cocontrols its regulon with WhiA to initiate developmental cell division in *Streptomyces*, MBio 7 (2016) (e00523-00516).

[73] K.J. Minch, T.R. Rustad, E.J. Peterson, J. Winkler, D.J. Reiss, S. Ma, M. Hickey, W. Brabant, B. Morrison, S. Turkarslan, C. Mawhinney, J.E. Galagan, N.D. Price, N.S. Baliga, D.R. Sherman, The DNA-binding network of *Mycobacterium tuberculosis*, Nat. Commun. 6 (2015) 5829.

[74] P.D. Facey, M.D. Hitchings, P. Saavedra-Garcia, L. Fernandez-Martinez, P.J. Dyson, R. Del Sol, Streptomyces coelicolor Dps-like proteins: differential dual roles in response to stress during vegetative growth and in nucleoid condensation during reproductive cell division, Mol. Microbiol 73 (2009) 1186–1202.

[75] Z.A. Ouafa, S. Reverchon, T. Lautier, G. Muskhelishvili, W. Nasser, The nucleoid-associated proteins H-NS and FIS modulate the DNA supercoiling response of the pel genes, the major virulence factors in the plant pathogen bacterium *Dickeya dadantii*, Nucleic Acids Res. 40 (2012) 4306–4319.

[76] Y. Ushijima, R.L. Ohniwa, A. Maruyama, S. Saito, Y. Tanaka, K. Morikawa, Nucleoid compaction by MrgA(Asp56Ala/Glu60Ala) does not contribute to staphylococcal cell survival against oxidative stress and phagocytic killing by macrophages, FEMS Microbiol. Lett. 360 (2014) 144–151.

[77] I.L. Bartek, L.K. Woolhiser, A.D. Baughn, R.J. Basaraba, W.R. Jacobs Jr., A.J. Lenaerts, M.I. Voskuil, *Mycobacterium tuberculosis* Lsr2 is a global transcriptional regulator required for adaptation to changing oxygen levels and virulence, MBio 5 (2014) e01106–e01114.

[78] D.J. Dwyer, D.M. Camacho, M.A. Kohanski, J.M. Callura, J.J. Collins, Antibiotic-induced bacterial cell death exhibits physiological and biochemical hallmarks of apoptosis, Mol. Cell 46 (2012) 561–572.

[79] J.A. Imlay, Iron-sulphur clusters and the problem with oxygen, Mol. Microbiol. 59 (2006) 1073–1082.